

¹ Drought, vegetation productivity, and land cover change in Chile

² Francisco Zambrano^{a,1,*}, Anton Vrielink^b, Francisco Fernández^c, Francisco Meza, Alejandro
³ Venegas-González, Iongel Duran-Llacer, Nicolas Raab, Dylan Craven

^a Universidad Mayor, Hémera Centro de Observación de la Tierra, Facultad de Ciencias, Escuela de Ingeniería en Medio Ambiente y Sustentabilidad, Santiago, Chile, 7500994

^b University of Twente, Faculty of Geo-Information Science and Earth Observation (ITC), Enschede, The Netherlands,

^c Universidad San Sebastian,

⁴ **Abstract**

Central Chile has been the focus of research studies due to the persistent decrease in water supply, which is impacting the hydrological system and vegetation development. This persistent period of water scarcity has been defined as a megadrought. Our objective is to assess the impact of drought on LULCC (land use land cover change) over continental Chile using drought indices of water supply and demand, soil moisture, and their impact on vegetation productivity. The monthly ERA5-Land (ERA5L) variables for precipitation, temperature, and soil moisture were used. From 2001 to 2022, we used the land cover MODIS product MCD12Q1, and from 2000 to 2023, we used the NDVI (Normalized Difference Vegetation Index) product MOD13A3 collection 6.1. As drought indices, we compute the standardized anomaly of cumulative NDVI (zcNDVI), the Standardized Precipitation Evapotranspiration Index (SPEI), the Evaporative Demand Drought Index (EDDI), and the Standardized Soil Moisture Index (SSI). These indices were calculated for time scales of 1, 3, 6, 12, 24, and 36 months, except for zcNDVI, which was for 6 months. We analyze the trend for LULCC, vegetation productivity, and drought indices. Also, we analyzed the temporal correlation of SPI, SPEI, EDDI, and SSI with zcNDVI to gain insights into the impact of water supply and demand on vegetation productivity. Our results showed that LULCC was highest in “Centro,” “Sur,” and “Austral,” with 36%, 31%, and 34% of change in the surface type, respectively. The EDDI shows that water demand has increased for all zones, with a major increase in “Norte Grande.” The drought indices of water supply and soil moisture evidence a decreasing trend, which decreases at longer time scales, from “Norte Grande” to “Sur.” “Austral” is the only zone that shows an increase in supply. Vegetation productivity measures by zcNDVI present a negative trend in “Norte Chico” and “Centro.” On the other hand, forests seem to be the most resistant to drought. The types that show to be most affected by variation in climate conditions are shrublands, savannas, and croplands. The drought indices that have the capability of explaining to a major degree the variance in vegetation productivity are SSI-12, followed by SPEI-24 and SPEI-12 in “Norte Chico” and “Centro.” The results indicate that “Norte Chico” and “Zona Central” are the most sensitive regions to water supply deficits lasting longer than a year. Our results can help develop a robust vegetation productivity forecasting model for land cover classes in Chile.

⁵ **Keywords:** drought, land cover change, satellite

*Corresponding author

Email addresses: francisco.zambrano@umayor.cl (Francisco Zambrano), a.vrielink@utwente.nl (Anton Vrielink), a.vrielink@utwente.nl (Francisco Fernández)

¹This is the first author footnote.

6 **1. Introduction**

7 Drought is often classified as meteorological when there is a decrease in precipitation below the mean
8 average of several years (more than 30 years), hydrological when these anomalies last for long periods (months
9 to years) and affect water systems, and agricultural when the deficit impacts plant health anomalies and
10 leads to decreased productivity (Wilhite and Glantz, 1985). However, it is important to note that drought
11 is also influenced by human activities, which were not considered in the definitions. Thus, Van Loon et al.
12 (2016) and AghaKouchak et al. (2021) have given an updated definition of drought for the Anthropocene,
13 suggesting that it should be considered the feedback of humans' decisions and activities that drives the
14 anthropogenic drought. Simultaneously, drought leads to heightened tree mortality and induces alterations
15 in land cover and land use, ultimately affecting ecosystems (Crausbay et al., 2017). Even though many
16 ecological studies have misinterpreted how to characterize drought, for example, sometimes considering
17 "dry" conditions as "drought" (Slette et al., 2019). Then, Crausbay et al. (2017) proposed the ecological
18 drought definition as "an episodic deficit in water availability that drives ecosystems beyond thresholds of
19 vulnerability, impacts ecosystem services, and triggers feedback in natural and/or human systems." In light
20 of current global warming, it is crucial to study the interaction between drought and ecosystems in order to
21 understand their feedback and impact on water security. (Bakker, 2012)

22 Human-induced greenhouse gas emissions have increased the frequency and/or intensity of drought as a
23 result of global warming, according to the sixth assessment report (AR6) of the Intergovernmental Panel
24 on Climate Change (IPCC) (Calvin et al., 2023). The evidence supporting this claim has been strengthened
25 since AR5 (IPCC, 2013). Recent studies, however, have produced contrasting findings, suggesting
26 that drought has not exhibited a significant trend over the past forty years. (Vicente-Serrano et al., 2022;
27 Kogan et al., 2020). Vicente-Serrano et al. (2022) analyzed the meteorological drought trend on a global
28 scale, finding that only in a few regions has there been an increase in the severity of drought. Moreover,
29 they attribute the increase in droughts over the past forty years solely to an increase in atmospheric evap-
30 orative demand (AED), which in turn enhances vegetation water demand, with important implications for
31 agricultural and ecological droughts. Also, they state that "the increase in hydrological droughts has been
32 primarily observed in regions with high water demand and land cover change". Similarly, Kogan et al.
33 (2020) analyzed the drought trend using vegetation health methods, finding that for the globe, hemispheres,
34 and main grain-producing countries, drought has not expanded or intensified for the last 38 years. Further,
35 the Masson-Delmotte (2021) suggests that there is a high degree of confidence that rising temperatures
36 will increase the extent, frequency, and severity of droughts. Also, AR6 (Calvin et al., 2023) predicts that
37 many regions of the world will experience more severe agricultural and ecological droughts even if global
38 warming stabilizes at 1.5°–2°C. To better evaluate the impact of drought trends on ecosystems, assessments
39 are needed that relate meteorological and soil moisture variables to their effects on vegetation.

40 From 1960 to 2019, land use change has impacted around one-third of the Earth's surface, which is four
41 times more than previously thought (Winkler et al., 2021). Multiple studies aim to analyze and forecast
42 changes in land cover globally (Winkler et al., 2021; Song et al., 2018) and regionally (Chamling and Bera,
43 2020; Homer et al., 2020; Yang and Huang, 2021). Some others seek to analyze the impact of land cover
44 change on climate conditions such as temperature and precipitation (Luyssaert et al., 2014; Pitman et al.,
45 2012). There is less research on the interaction between drought and land cover change (Chen et al., 2022;
46 Akinyemi, 2021; Peng et al., 2017). Peng et al. (2017) conducted a worldwide investigation utilizing net
47 primary production to examine the spatial and temporal variations in vegetation productivity at global
48 level. The study aimed to assess the influence of drought by comparing the twelve-month Standardized
49 Precipitation Evapotranspiration Index (SPEI) and land cover change. According to their findings, drought
50 is responsible for 37% of the decline in vegetation productivity, while water availability accounts for 55% of
51 the variation. Chen et al. (2022) studied the trend of vegetation greenness and productivity and its relation
52 to meteorological drought (SPEI of twelve months in December) and soil moisture at the global level. The
53 results showed lower correlations (<0.2) for both variables. Akinyemi (2021) evaluates drought trends and
54 land cover change using vegetation indices in Botswana in a semi-arid climate. These studies mostly looked
55 at how changes in land cover and vegetation productivity are related to a single drought index (SPEI) over

56 a single time period of 12 months. SPEI takes into account the combined effect of precipitation and AED as
57 a water balance, but it does not allow us to know the contribution of each variable on its own. Some things
58 worth investigating in terms of land cover change and vegetation productivity are: i) How do they respond
59 to short- to long-term meteorological droughts? ii) How do they behave in humid and arid climatic zones
60 regarding drought? And iii) What is the role of soil moisture? Likewise, there is a lack of understanding of
61 how the alteration in water supply and demand is affecting land cover transformations.

62 Chile's diverse climatic and ecosystem types ([Beck et al. \(2023\)](#); [Luebert and Plisoff \(2022\)](#)) make it an
63 ideal natural laboratory for studying climate and ecosystems. Additionally, the country has experienced
64 severe drought conditions that have had significant effects on vegetation and water storage. Central Chile
65 faced a persistent precipitation deficit between 2010 and 2022, defined as a megadrought ([Garreaud et al.,](#)
66 [2017](#)), which has impacted the Chilean ecosystem. This megadrought was defined by the Standardized
67 Precipitation Index (SPI) of twelve months in December having values below one standard deviation. Some
68 studies have addressed how this drought affects single ecosystems in terms of forest development ([Miranda](#)
69 [et al., 2020](#); [Venegas-González et al., 2018](#)), forest fire occurrence ([Urrutia-Jalabert et al., 2018](#)), and crop
70 productivity ([Zambrano, 2023](#); [Zambrano et al., 2018, 2016](#)). We found one study regarding land cover and
71 drought in Chile. The study by [Fuentes et al. \(2021\)](#) evaluates water scarcity and land cover change in Chile
72 between 29° and 39° of south latitude. [Fuentes et al. \(2021\)](#) used the SPEI of one month for evaluating
73 drought, which led to misleading results. For example, they did not find a temporal trend in the SPEI but
74 found a decreasing trend in water availability and an increase trend on AED, which in turn should have been
75 capable of being captured with longer time scales of the SPEI. The term "megadrought" in Chile is used to
76 describe a prolonged water shortage that lasts for several years, resulting in a permanent deficit that impacts
77 the hydrological system ([Boisier et al., 2018](#)). Hence, it is imperative to assess temporal scales that take into
78 account the cumulative effect within some years. There is little knowledge about the relationship between
79 drought and ecosystem in Chile; thus, it is important to understand in more detail how meteorological and
80 soil moisture droughts influence ecosystem dynamics to inform adaptation options.

81 A detailed spatiotemporal assessment of the interaction of drought for short- to long-term and land cover
82 change requires information on vegetation as well as weather variables such as precipitation, temperature,
83 and soil moisture. Weather networks in Chile present some disadvantages, such as spatio-temporal gaps, a
84 short history, and irregular quality, which make them difficult to represent the whole extent of the country
85 spatially. In order to do this, we use reanalysis data from ERA5-Land ([Muñoz-Sabater et al., 2021](#)) to create
86 drought indices that consider AED, precipitation, and soil moisture over a range of time periods, from the
87 short to the long term. Also, we use vegetation spectral information and annual land cover change from
88 the Moderate-Resolution Imaging Spectroradiometer (MODIS). We expect to gain insight regarding the
89 temporal evolution of water demand, water supply, and soil moisture, as well as the interaction with land
90 cover change and vegetation productivity. Here, we analyze the multi-dimensional impacts of drought across
91 ecosystems in continental Chile. More specifically, we aim to assess: i) temporal changes in land-use cover
92 and the direction and magnitude of their relationships with drought indices for water demand and supply,
93 soil moisture, and vegetation productivity; ii) short- to long-term temporal trends in multi-scalar drought
94 indices; and iii) the relationship between vegetation productivity and drought indices for water demand and
95 supply and soil moisture across Chilean ecosystems.

96 2. Study area

97 Continental Chile has a diverse climate conditions with strong gradients from north to south and east
98 to west ([Aceituno et al., 2021](#)) (Figure 1 a), which determines its great ecosystem diversity ([Luebert and](#)
99 [Plisoff \(2022\)](#)) (Figure 1 c). The Andes Mountains are a main factor in climate latitudinal variation
100 ([Garreaud, 2009](#)). In order to characterize the climate and ecosystem of Chile, we utilize the Köppen-Geiger
101 classification system developed by [Beck et al. \(2023\)](#) and the land cover data derived from the MODIS
102 product for the period of 2001–2022, based on the International Geosphere-Biosphere Programme (IGBP)
103 classification scheme proposed by [Friedl and Sulla-Menashe \(2019\)](#). "Norte Grande" and "Norte Chico"
104 predominate in an arid desert climate with hot (Bwh) and cold (Bwk) temperatures. At the south of "Norte"

105 Chico,” the climate changes to an arid steppe with cold temperatures (Bsk). In these two northern regions,
 106 the land is mostly bare, with a minor surface of vegetation types such as shrubland and grassland. In the
 107 zones “Centro” and the north half of “Sur,” the main climate is Mediterranean, with warm to hot summers
 108 (Csa and Csb). Land cover in “Centro” comprises a significant amount of shrubland and savanna (50%),
 109 grassland (16%), forest (8%), and croplands (5%). An oceanic climate (Cfb) predominates in the south
 110 of “Sur” and the north of “Austral.” Those zones are high in forest and grassland. The southern part of
 111 the country has a tundra climate, and in “Austral”, it is a cold semi-arid area with an extended surface of
 112 grassland, forest, and, to a lesser extent, savanna.

113 3. Materials and Methods

114 3.1. Software and packages used

115 For the downloading, processing, and analysis of the spatio-temporal data, we used the open source software
 116 for statistical computing and graphics, R ([R Core Team, 2023](#)). For downloading ERA5L, we used the
 117 `{ecmwfr}` package ([Hufkens et al., 2019](#)). For processing raster data, we used `{terra}` ([Hijmans, 2023](#)) and
 118 `{stars}` ([Pebesma and Bivand, 2023](#)). For managing vectorial data, we used `{sf}` ([Pebesma, 2018](#)). For
 119 the calculation of AED, we used `{SPEI}` ([Beguería and Vicente-Serrano, 2023](#)). For mapping, we use `{tmap}`
 120 ([Tennekes, 2018](#)). For data analysis, the suite `{tidyverse}` ([Wickham et al., 2019](#)) was used.

121 3.2. Data

122 3.2.1. Earth observation data

123 For water supply and demand variables, we used ERA5L ([Muñoz-Sabater et al., 2021](#)), a reanalysis dataset
 124 that provides the evolution of land variables since 1950. It has a spatial resolution of 0.1°, hourly frequency,
 125 and global coverage. We selected the variables for total precipitation, 2 meter temperature maximum and
 126 minimum, and volumetric soil water layers between 0 and 100cm of depth (layer 1 to layer 3). The data
 127 was downloaded using the Copernicus Climate Data Store (CDS) Application Program Interface (API)
 128 implemented in `{ecmfwr}` ([Hufkens et al., 2019](#)).

129 To derive a proxy for vegetation productivity, we used the product MOD13A3 collection 6.1 from MODIS
 130 ([Didan, 2015](#)). It provides vegetation indices (NDVI and EVI) at 1km of spatial resolution and monthly
 131 frequency. The MOD13A3.061 and MCD12Q1.061 were retrieved from the online Data Pool, courtesy of
 132 the NASA EOSDIS Land Processes Distributed Active Archive Center (LP DAAC), USGS Earth Resources
 133 Observation and Science (EROS) Center, Sioux Falls, South Dakota, <https://lpdaac.usgs.gov/tools/data-pool/>.

Table 1: Description of the earth observation data used

Product	Sub-product	Variable	Spatial Resolution	Period	Units	Short Name	
ERA5L		Precipitation	0.1°	1981-2023	mm	P	
		Maximum temperature			°C	T _{max}	
		Minimum temperature			°C	T _{min}	
		Volumetric Soil Water Content at 1m			m3/m3	SM	
ERA5L*	MOD13A3.061	Atmospheric Evaporative Demand	0.1°	1981-2023	mm	AED	
MODIS		Normalized Difference Vegetation Index	1 km	2000-2023		NDVI	
		land cover IGBP scheme		2001-2022		land cover	

*Derived from ERA5L with Eq. 1.

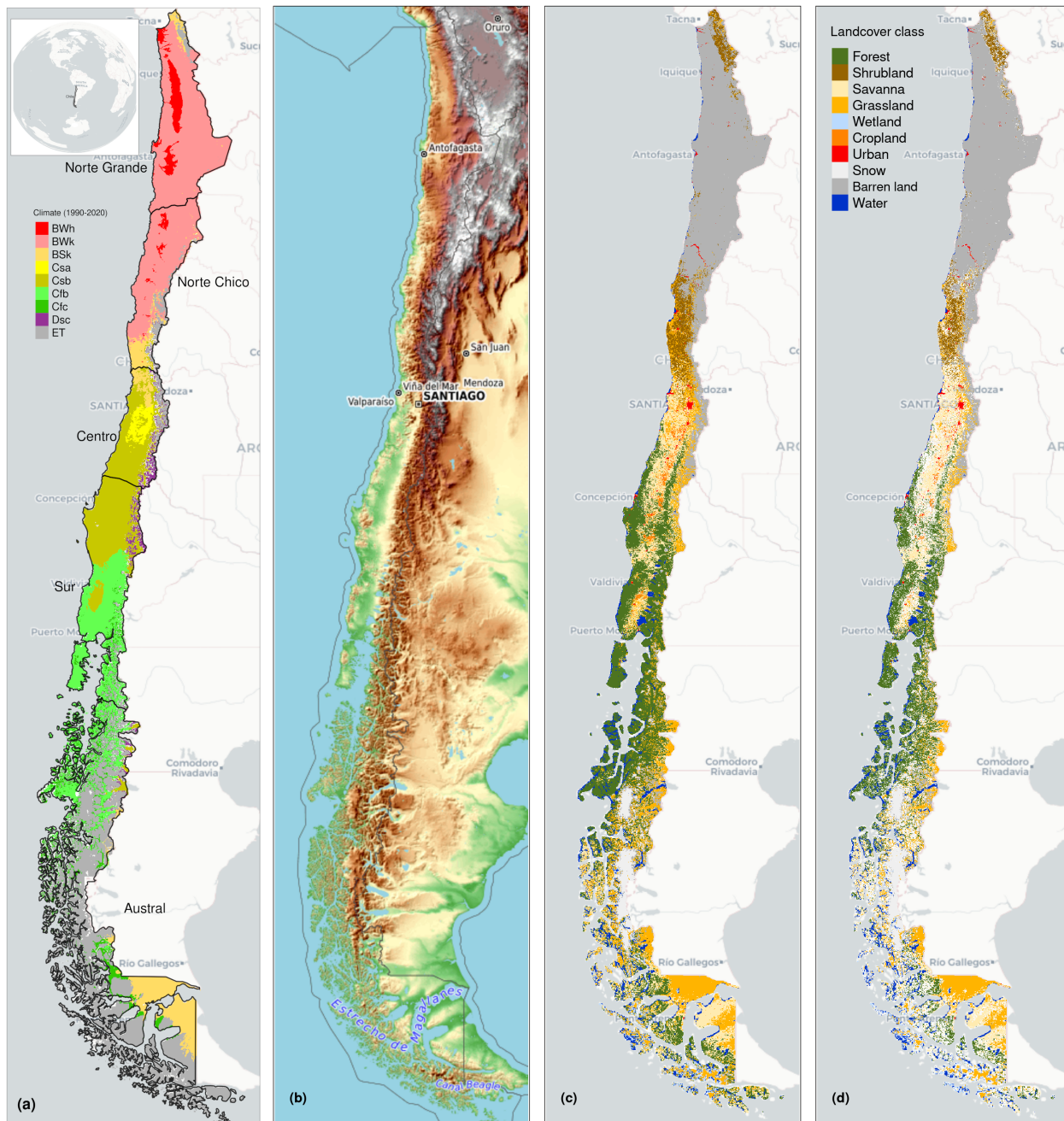


Figure 1: (a) Chile with the Koppen-Geiger climate classes and the five macrozones “Norte Grande”, “Norte Chico”, “Centro”, “Sur”, and “Austral”. (b) Topography reference map. (c) land cover classes for 2022. (d) Persistent land cover classes (> 80%) for 2001-2022

135 *3.2.2. Weather stations*

136 We compared the ERA5L variables for monthly mean temperature, total precipitation, and volumetric soil
 137 water content against values retrieved by weather stations. For temperature and precipitation, we used the
 138 weather network from the Ministry of Agriculture of Chile (www.agromet.com) between 2015 and 2023. We
 139 used 277 stations located throughout Chile. For soil moisture, we select a private soil network that is owned

¹⁴⁰ by the agricultural enterprise Garces Fruit, which has 99 stations in Central Chile, located in cherry fruit
¹⁴¹ crops. The sensors are installed at 30, 60, and 90m and are the model Teros 12 from MeterGroup. To avoid
¹⁴² the effect of irrigation on soil moisture, which ERA5L hardly captures, we used daily data for the year 2022
¹⁴³ and the months outside the growing season, May to September.

¹⁴⁴ *3.2.3. Validation of ERA5L variables*

¹⁴⁵ To account for the performance of the ERA5L climatic variables regarding the values measured by the
¹⁴⁶ weather stations. We selected the following metrics:

$$MAE = \frac{1}{n} \sum |E - S|$$

$$Bias = \frac{\sum E}{\sum S}$$

$$ubRMSE = \sqrt{\frac{\sum [(E_i - \bar{E}) - (S_i - \bar{S})]^2}{n}}$$

$$CC = \frac{\sum (S_i - \bar{S})(E_i - \bar{E})}{\sqrt{(S_i - \bar{S})^2(E_i - \bar{E})^2}}$$

¹⁴⁹ *MAE*: mean absolute error *bias*: bias *ubRMSE*: unbiassed root mean squared error *CC*: coefficient of
¹⁵⁰ correlation *S*: value of the variable measure by the weather station *E*: value of the variable measure by
¹⁵¹ ERA5L

¹⁵² *3.3. Drought Indices*

¹⁵³ *3.3.1. Atmospheric Evaporative Demand (AED)*

¹⁵⁴ For the indices EDDI and SPEI that use water demand, first we have to calculate the AED. For this, we
¹⁵⁵ used the method of Hargreaves ([Hargreaves, 1994](#); [Hargreaves and Samani, 1985](#)):

$$AED = 0.0023 \cdot Ra \cdot (T + 17.8) \cdot (T_{max} - T_{min})^{0.5} \quad (1)$$

¹⁵⁶ where *Ra* ($MJ m^2 day^{-1}$) is extraterrestrial radiation; *T*, *T_{max}*, and *T_{min}* are mean, maximum, and
¹⁵⁷ minimum temperature ($^{\circ}C$). We calculate the centroid coordinates per pixel and use the latitude to estimate
¹⁵⁸ *Ra*.

¹⁵⁹ We chose the method of Hargreaves to estimate AED because of its simplicity, which only requires tem-
¹⁶⁰ peratures and extrarrestrial radiation. Also, it has been recommended over other methods when the use of
¹⁶¹ several climatic variables is limited ([Vicente-Serrano et al., 2014](#)).

¹⁶² *3.3.2. Non-parametric calculation of drought indices*

¹⁶³ We derived the drought indices of water supply and demand, soil moisture from the ERA5L dataset, and
¹⁶⁴ vegetation from the MODIS product, all at monthly frequency.

¹⁶⁵ To evaluate water demand, we chose the *EDDI* ([Hobbins et al., 2016](#); [McEvoy et al., 2016](#)) index, which
¹⁶⁶ uses the *AED*. We used the *SPI* ([McKee et al., 1993](#)), a drought monitoring index that the World Me-
¹⁶⁷ teorological Organization (WMO) recommends. We calculated the *SPEI*, which used a balance between
¹⁶⁸ *P* and *AED*, in this case, an auxiliary variable *D* = *P* − *AED* is used. In this study, we used the *SSI*
¹⁶⁹ (standardized soil moisture index at 1 m) ([Hao and AghaKouchak, 2013](#); [AghaKouchak, 2014](#)), which uses
¹⁷⁰ soil moisture at 1m depth. Finally, for the proxy of productivity, *zcNDVI*, we used the NDVI. Before

¹⁷¹ using the NDVI, it was smoothed using a locally weighted polynomial regression, following the procedure
¹⁷² described in [Zambrano et al. \(2018\)](#) and [Zambrano et al. \(2016\)](#).

¹⁷³ All the indices are multi-scalar and were calculated for time scales of 1, 3, 6, 12, 24, and 36 months, except
¹⁷⁴ for zcNDVI, which was calculated for 6 months. The goal is to be able to evaluate short- and long-term
¹⁷⁵ droughts in water demand and supply and soil moisture. This is particularly important for central Chile
¹⁷⁶ because it has suffered from a prolonged decrease in precipitation for more than 12 years ([Garreaud et al.,](#)
¹⁷⁷ [2020](#); [Boisier et al., 2018](#); [Garreaud et al., 2017](#)).

¹⁷⁸ To calculate the drought indices, first we must calculate the accumulation of the variable. In this case, for
¹⁷⁹ generalization purposes, we will use V , referring to P , AED , D , $NDVI$, and SM (Table 1). We cumulated
¹⁸⁰ each V over the time series of n values, and for the time scales s :

$$A_{si} = \sum_{i=n-s-i+2}^{n-i+1} V_i \quad \forall i \geq n - s + 1 \quad (2)$$

¹⁸¹ It corresponds to a moving window (convolution) that sums the variable for s starting for the last month
¹⁸² n until the month, which could sum for s months ($n-s+1$). Once the variable is cumulated over time
¹⁸³ for the scale s , we used a nonparametric approach following [Hobbins et al. \(2016\)](#) to derive the drought
¹⁸⁴ indices. Thus, the empirically derived probabilities are obtained through an inverse normal approximation
¹⁸⁵ ([Abramowitz and Stegun, 1968](#)). Then, we used the empirical Tukey plotting position ([Wilks, 2011](#)) over
¹⁸⁶ A_i to derive the $P(A_i)$ probabilities across a period of interest:

$$P(A_i) = \frac{i - 0.33}{n + 0.33} \quad (3)$$

¹⁸⁷ The drought indices SPI , $SPEI$, $EDDI$, SSI , and $zcNDVI$ are obtained following the inverse normal
¹⁸⁸ approximation:

$$DI(A_i) = W - \frac{C_0 + C_1 \cdot W + c_2 \cdot W^2}{1 + d_1 \cdot W + d_2 \cdot W^2 + d_3 \cdot W^3} \quad (4)$$

¹⁸⁹ DI is referring to the drought index calculated for the variable V . The values for the constants are:
¹⁹⁰ $C_0 = 2.515517$, $C_1 = 0.802853$, $C_2 = 0.010328$, $d_1 = 1.432788$, $d_2 = 0.189269$, and $d_3 = 0.001308$. For
¹⁹¹ $P(A) \leq 0.5$, $W = \sqrt{-2 \cdot \ln(P(A_i))}$, and for $P(A_i) > 0.5$, replace $P(A_i)$ with $1 - P(A_i)$ and reverse the sign
¹⁹² of $DI(A_i)$.

¹⁹³ 3.4. LULC change for 2001-2022 and its relation with water supply and demand, and soil moisture

¹⁹⁴ 3.4.1. Land cover macroclases and validation

¹⁹⁵ To analyze the LULCC, we use the IGBP scheme from the MCD12Q1 collection 6.1 from MODIS. This
¹⁹⁶ product has a yearly frequency from 2001 to 2022. The IGBP defines 17 classes; from these, we regrouped
¹⁹⁷ into ten macroclasses, as follows: classes 1-4 to forest, 5-7 to shrublands, 8-9 to savannas, 10 as grasslands,
¹⁹⁸ 11 as wetlands, 12 and 14 to croplands, 13 as urban, 15 as snow and ice, 16 as barren, and 17 to water
¹⁹⁹ bodies. Thus, we have a land cover raster time series with the ten classes for 2001 and 2023.

²⁰⁰ To validate the land cover obtained, we compare the macroclasses with the ones of a more detailed land
²⁰¹ cover map made by [Zhao et al. \(2016\)](#) for Chile with samples acquired in the years 2013–2014 (LCChile).
²⁰² The later has a spatial resolution of 30 m and three levels of defined classes; from those, we used level 1,
²⁰³ which fits with the macroclasses land cover. We chose the years 2013 (IGBP2013) and 2014 (IGBP2014)
²⁰⁴ from land cover macrolcasses to validate with LCChile.

²⁰⁵ We follow the next procedure:

- 206 i) resampled LCChile to the spatial resolution (500m) of the land cover macroclasses using the nearest
 207 neighbor method,
 208 ii) took a random sample of 1000 points within continental Chile and extracted the classes that fell within
 209 each point for LCChile, IGBP2013, and IGBP2014; we considered the point extracted from LCChile
 210 as the truth and the values from the other two years as predictions.
 211 iii) calculate a confusion matrix with the classes extracted from the 1000 points for LCChile, IGBP2013,
 212 and IGBP2014. Calculate the performance metrics of accuracy and F1.

$$213 \quad Accuracy = \frac{TP + TN}{TP + TN + FP + FN} = \frac{\text{correct classifications}}{\text{all classifications}}$$

$$F1 = \frac{2 \cdot TP}{2 \cdot TP + FP + FN}$$

214 where TP and FN refer to true positive and false negative, correctly classified classes; TN and FP to true
 215 negative and false positive, wrongly classified classes.

216 3.4.2. Land cover persistence mask 2001–2022

217 Climate, vegetation development, seasonality, and changes in vegetation type all have an impact on the
 218 time series of NDVI. In this study, we want to examine the variation in vegetation productivity across various
 219 land cover types and how water demand, water supply, and soil moisture affect it. In order to avoid changes
 220 due to a change in the land cover type that will wrongly impact NDVI, we will develop a persistence mask
 221 for land cover for 2001–2023. Thereby, we reduce an important source of variation on a regional scale.

222 Therefore, we generated a raster mask for IGBP MODIS per pixel using macroclasses that remain constant
 223 for at least 80% of the years (2001–2022). This enables us to identify regions where the land cover of the
 224 macroclasses has remained constant.

225 3.4.3. Land cover trend and drought indices

226 We calculated the surface occupied per land cover class into the five macrozones (“Norte Grande” to
 227 “Austral”) per year for 2001–2023. After that, we calculated the trend’s change in surface; we used the Sen’
 228 slope (Sen, 1968) based on Mann-Kendall (Kendall, 1975). This way, we obtain a matrix of trends of 5 x 5
 229 (macrozones x land cover). The aim is to later explore if the trend in land cover classes is associated with
 230 a trend in the drought indices. For this, we will use the techniques of regression and regularization of Lasso
 231 (Tibshirani et al., 2010) and Ridge (Hoerl and Kennard, 1970). Also, we will test random forests for this
 232 purpose (Ho, 1995). We will choose the trend of land cover surface per macroclass and macrozone as the
 233 response variable and the trend of the drought indices (SPI, SPEI, EDDI, and SSI for time scales 1, 3, 6, 12,
 234 24, and 36 months) as the predictor variables. With this analysis, we expect to gather insights regarding
 235 whether there is a pattern of climatic influence along Chile or if what is happening in Central Chile has to
 236 do with more localized climatic conditions.

237 3.5. Trend of drought indices for water demand and supply, soil moisture, and vegetation productivity

238 3.5.1. Mann-Kendall and Sen’s slope

239 To estimate if there are significant positive or negative trends for the drought indices, we used the non-
 240 parametric test of Mann-Kendall (Kendall, 1975). To determine the magnitude of the trend, we used Sen’s
 241 slope (Sen, 1968). Some of the advantages of applying this methodology are that the Sen’s slope is not
 242 affected by outliers as regular regression does, and it is a non-parametric method that is not affected by the
 243 distribution of the data. We applied both to the six time scales from 1981 to 2023 (monthly frequency) and
 244 the indices SPI, EDDI, SPEI, and SSI. In the case of zcNDVI (six months) was for 2000 to 2023. Thus, we
 245 have 31 trends. Also, we extracted the trend aggregated by macrozone and land cover class, obtaining a
 246 table of 31x5x5 (drought indices trends x macrozone x land cover class). We will use this data in Section 3.4
 247 to analyze if there is a strong relationship between the trends of drought indices and land cover surface
 248 within continental Chile.

249 *3.5.2. Trend in vegetation productivity without land cover change*

250 ? made a global analysis of the drought's severity trend using SPI, SPEI, and the Standardized Evapo-
251 transpiration Deficit Index (SEDI; [Vicente-Serrano et al. \(2018\)](#)) to evaluate AED. They indicate that the
252 increase in hydrological drought has been due to anthropogenic effects rather than climate change. This is
253 because the global increase in AED did not explain the change in the spatial pattern of the hydrological
254 drought. Also, they state that "*the increase in hydrological droughts has been primarily observed in regions*
255 *with high water demand and land cover change*". We will contrast this hypothesis with what is occurring
256 in Chile. To achieve this, we will use the land cover class type that remains more than 80% of types for
257 2001–2022 to evaluate the trend on zcNDVI and use this as a mask where there are low changes.

258 *3.6. Impact for water supply and demand, and soil moisture in vegetation productivity within land cover*
259 *types*

260 We analyze the drought indices of water demand and supply and soil moisture against vegetation to address:
261 i) if short- or long-term time scales are most important in impacting vegetation through Chile; and ii) the
262 strength of the correlation for the variable and the time scale. Then, we will summarize for each land cover
263 class and macrozone. Thus, we will be able to advance in understanding how climate is affecting vegetation,
264 considering the impact on the five macroclasses of vegetation: forest, cropland, grassland, savanna, and
265 shrubland.

266 An analysis is conducted on the linear correlation between the indices SPI, SPEI, EDDI, and SSI over time
267 periods of 1, 3, 6, 12, 24, and 36 months, and zcNDVI. The objective is to determine the impact of soil
268 moisture and water demand and supply on vegetation productivity. We implemented a methodology similar
269 to that of [Meroni et al. \(2017\)](#) when comparing the SPI for meteorological drought to the cumulative FAPAR
270 (Fraction of Absorbed Photosynthetically Active Radiation), which served as an indicator for vegetation
271 productivity. A pixel-to-pixel linear correlation analysis was performed for each index. To begin, the
272 Pearson coefficient of correlation is computed for each of the six time scales. A significant time scale is
273 identified as the one that attains the highest correlation ($p < 0.05$). Subsequently, the Pearson correlation
274 coefficient corresponding to the time scales at which the value peaked was extracted. As a result, for each
275 index, we generated two raster maps: one containing the time scales and the other the correlation value.

276 **4. Results**

277 *4.1. Data*

278 *4.1.1. Validation of ERA5L variables*

279 The average metrics of performance of ERA5L over the 266 weather stations were in the case of monthly
280 temperature: $ubRMSE = 1.06^{\circ}\text{C}$, $MAE = 1.131^{\circ}\text{C}$, and $CC = 0.963$, showing a good agreement, low
281 error, and low overestimation. For cumulative monthly precipitation, $MAE = 28.1 \text{ mm}$, $bias = 1.93$, and
282 $CC = 0.845$, showing a high correlation and a 93% bias and being overestimated by ERA5L. In the case
283 of the 97 soil moisture stations, we averaged for the three depths (30, 60, and 90m) and then compared
284 it with volumetric water content at 1m derived from ERA5L. For this case, we made a daily comparison,
285 having a $CC = 0.71$, $RMSE = 0.174 \text{ m}^3\text{m}^{-3}$, $MAE = 0.167 \text{ m}^3\text{m}^{-3}$, and $bias = 1.74$. The ERA5 soil
286 moisture overestimate is 74%, but it has a kind of good correlation. For more detailed information, consult
287 the supplementary material (SSX).

288 *4.2. LULC change for 2001-2022 and its relation with water supply and demand, and soil moisture*

289 *4.2.1. Land cover macroclases and validation*

290 For vegetation, we obtained and use hereafter five macroclasses of land cover from IGBP MODIS: forest,
291 shrubland, savanna, grassland, and croplands. Figure 1 c shows the spatial distribution of the macroclasses
292 through Chile for the year 2022. The validation of IGBP2013 and IGBP2014 with LCChile reached near
293 the same metrics of performance, having an accuracy of ~0.82 and a F1 score of ~0.66 (see SS1).

294 4.2.2. Land cover persistence mask 2001-2022

295 Figure 1 d, shows the macroclasses of land cover persistance (80%) during 2021-2022, respectively (2).
 296 Within continental Chile, forest is the vegetation type with the highest surface area at $135,00 \text{ km}^2$, followed
 297 by grassland ($73,176 \text{ km}^2$), savanna ($54,410 \text{ km}^2$), shrubland ($24,959 \text{ km}^2$), and cropland ($3,100 \text{ km}^2$) (Table
 298 2). The macrozones with major LULCC for 2001–2022 were “Centro,” “Sur,” and “Austral” with 36%, 31%,
 299 and 34%, respectively (Figure 1 and Table 3); of its surface that changes the type of land cover. Figure 2
 300 shows the summary of the proportion of surface per land cover class and macrozone, derived from the
 301 persistance mask over continental Chile.

Table 2: Surface of the land cover class that persist during 2001-2022

macrozone	Surface [km ²]					
	Forest	Cropland	Grassland	Savanna	Shrubland	Barren land
Norte Grande			886		7,910	171,720
Norte Chico		90	4,283	589	16,321	84,274
Centro	3,739	1,904	7,584	19,705	844	12,484
Sur	72,995	1,151	7,198	15,906		2,175
Austral	60,351		54,297	19,007	249	7,218
Total	—	137,085	3,145	74,247	55,206	25,324
						277,870

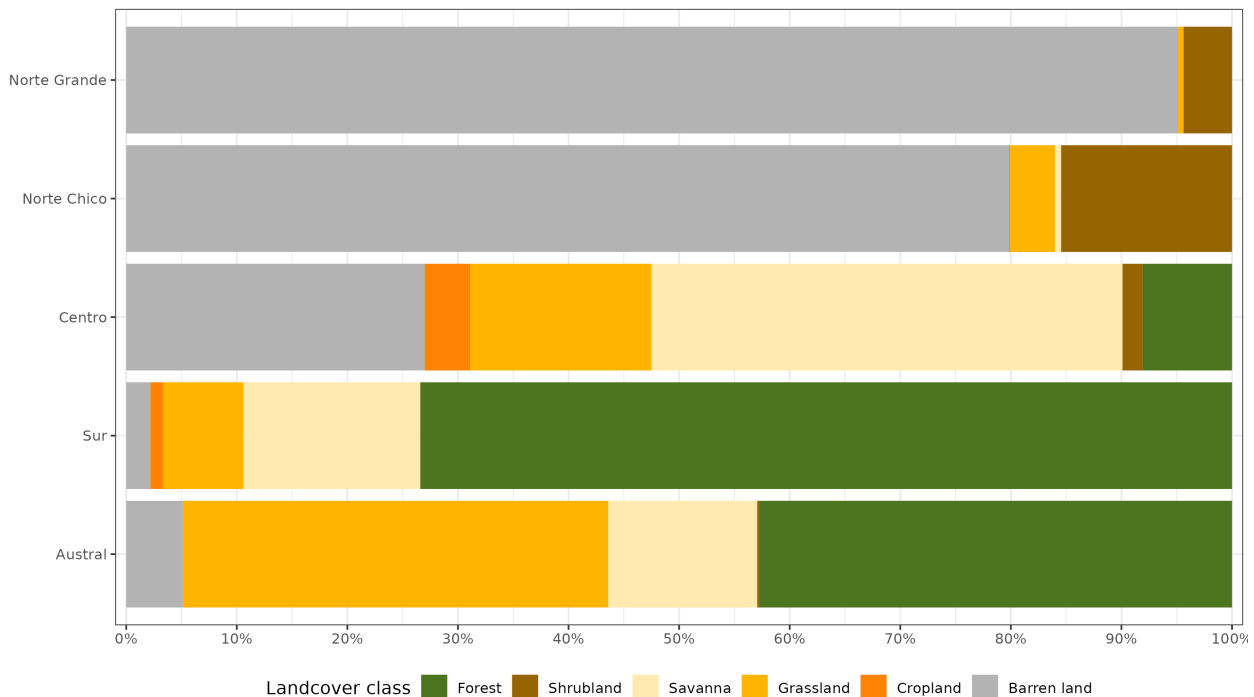


Figure 2: Proportion of land cover class from the persistent land cover for 2001-2022 (>80%) per macrozone

302 4.2.3. Land cover trend and drought indices

303 The “Norte Chico” shows an increase in barrend land of $111 \text{ km}^2 \text{ year}^{-1}$ and a reduction in the class
 304 savanna of $70 \text{ km}^2 \text{ year}^{-1}$. In the “Centro” and “Sur,” there are changes in the Chilean matorral, with an
 305 important reduction in savanna (136 to $318 \text{ km}^2 \text{ yr}^{-1}$), and an increase in shrubland and grassland. Showing
 306 a change for more dense vegetation types. It appears to be a shift in the area of cropland from the “Centro”
 307 to the “Sur.” Also, there is a high increase in forest ($397 \text{ km}^2 \text{ yr}^{-1}$) in the “Sur,” replacing the savanna lost.

Table 3: The value of Sen's slope trend next to the time-series plot of surface per land cover class (IGBP MCD12Q1.016) for 2001–2022 through Central Chile. Values of zero indicate that there was not a significant trend. Red dots on the plots indicate the maximum and minimum values of surface.

macrozone	Trend of change [$\text{km}^2 \text{ year}^{-1}$]											
	Forest		Cropland		Grassland		Savanna		Shrubland		Barren land	
	x	y	x	y	x	y	x	y	x	y	x	y
Norte Grande								0.0			0.0	0.0
Norte Chico					-12.1			0.0		-70.0		111.2
Centro		0.0			-22.4		83.2		-136.2		146.0	22.9
Sur		396.6			37.8		0.0		-318.8			0.0
Austral		0.0					0.0		172.1		-36.9	-93.2

308 Further, we want to address whether the trend in land cover change for 2001–2023 is associated with
 309 trends in drought indices of water demand and supply and/or soil moisture for macrozone and land cover
 310 macroclasses. From the three methods tested, Ridge, Lasso, and Random Forest, neither gives significant
 311 results regarding whether the trend in a drought index for any time scale explains the trend in land cover
 312 change. Nevertheless, in “Norte Chico” and “Centro,” there is a decrease in croplands and savanna and an
 313 increase in barren land, which is associated with the variation in drought indices. Mainly for a decrease in
 314 water supply (SPI and SSI) and an increase in water demand (EDDI). However, due to the high variability
 315 from north to south in Chile, the climatic conditions (arid, semi-arid, and humid), and the land cover type,
 316 we believe that only in those zones could the LULCC be driven to some degree by drought.

317 4.3. Trend of drought indices for water demand and supply, soil moisture, and vegetation productivity

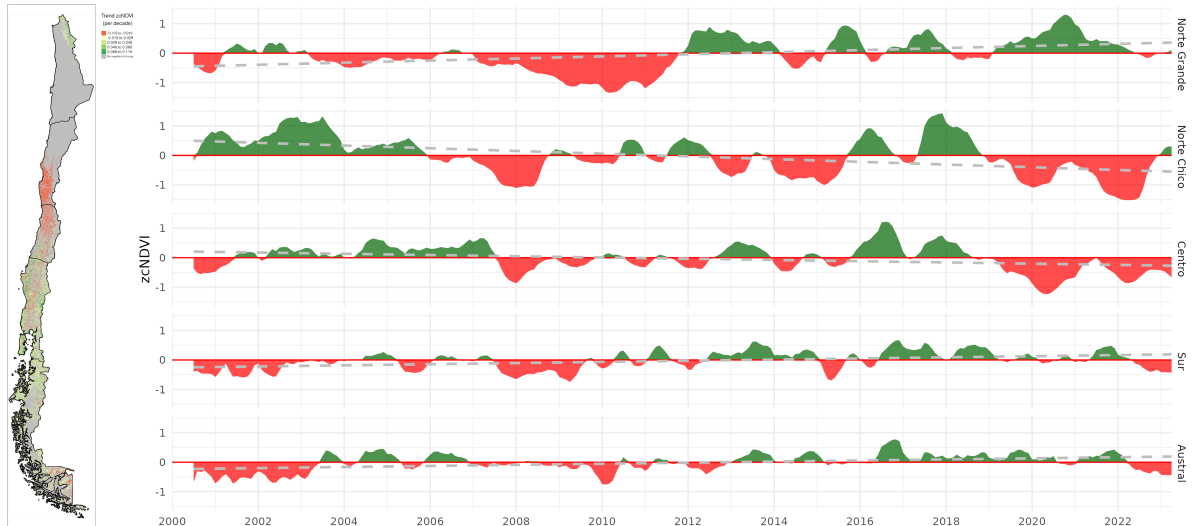


Figure 3: (a) Map of the linear trend of the index zcNDVI-6 for 2001–2023. Greener colors indicate a positive trend; redder colors correspond to a negative trend and a decrease in vegetation productivity. Grey colors indicate either no vegetation or a change in land cover type for 2001–2022. (b) Temporal variation of zcNDVI-6 aggregated at macrozone level within continental Chile. Each horizontal panel corresponds to a macrozone from ‘Norte Grande’ to ‘Austral’.

318 In “Norte Grande,” vegetation productivity, as per the z-index, exhibits a yearly increase of 0.02 in the
 319 five land cover macroclasses, with respect to grassland and shrubland categories. There is a negative trend
 320 in “Norte Chico” with -0.04 and “Centro” with -0.02 per decade. In the “Norte Chico,” savanna (-0.05) has
 321 the lowest trend, and the rest of the types are around -0.04. In “Centro,” shrubland reaches -0.06, grassland

322 -0.05, and croplands and savanna -0.01 per decade. This could be associated either with a reduction in
 323 vegetation surface, a decrease in biomass, or browning ([Miranda et al., 2023](#)). Vegetation reached its lowest
 324 values since the year 2019, reaching an extreme condition in early 2020 and 2022 in the “Norte Chico”
 325 and Centro” (Mega Drought). The “Sur” and “Austral” show a positive trend of around 0.016 per decade
 326 (Figure 3). Despite the croplands suffering from drought just as badly as the native vegetation in “Norte
 327 Chico,” the Chilean matorral ([Fuentes et al., 2021](#)) appears to be the region most affected by a negative
 328 trend in vegetation productivity.

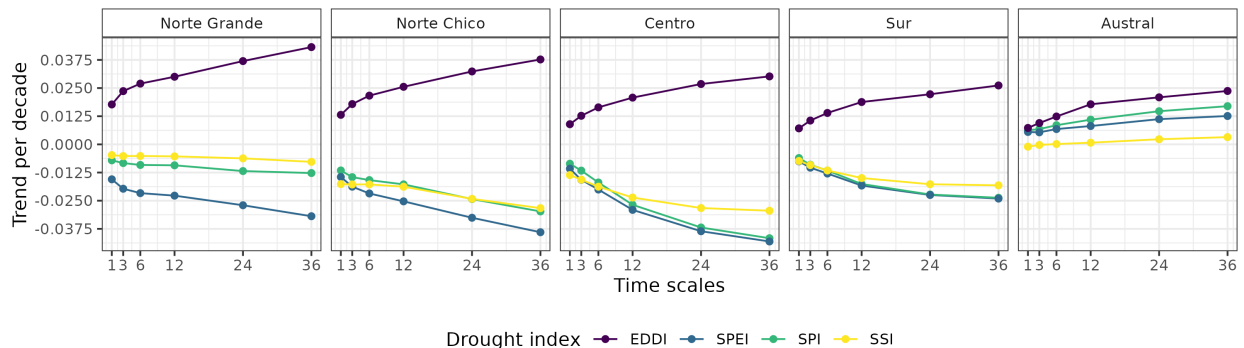


Figure 4: Trend per decade for the drought indices SPI, EDDI, SPEI, and SSI aggregated by macrozone.

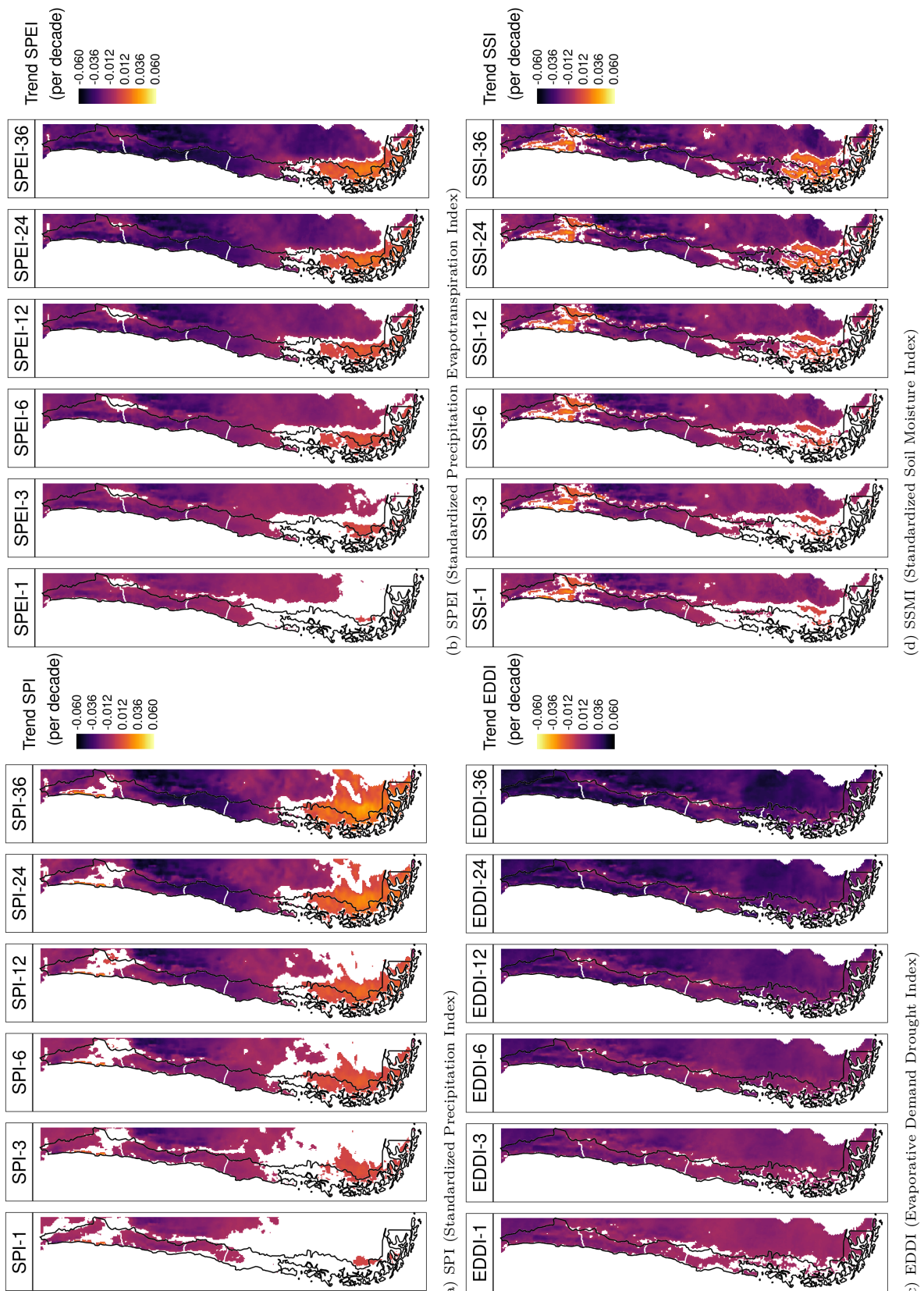
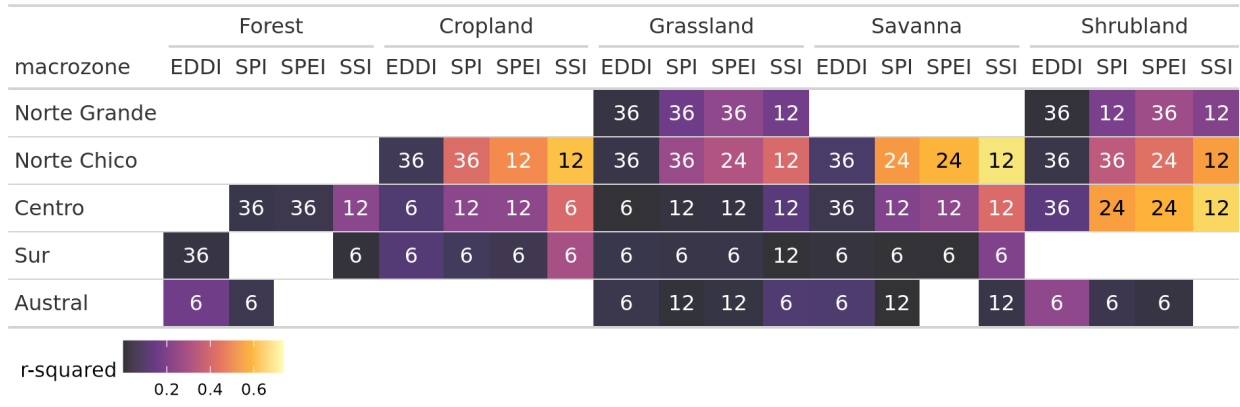


Figure 5: Linear trend of the drought index (*) at time scales of 1, 3, 6, 12, 24, and 36 months for 1981-2023

Table 4: Summary per land cover macroclass and macrozone regarding the correlation between zcNDVI with the drought indices EDDI, SPI, SPEI, and SSI for time scales of 1, 3, 6, 12, 24, and 36. The numbers in each cell indicate the time scale that reached the maximum correlation for the land cover and macrozone, and the color indicates the strength of the r-squared obtained with the index and the time scale.



329 Analyzing the water supply, the macrozones that have the lowest trend are “Norte Chico” and “Centro,”
330 where the SPI, SPEI, and SSI show that it decreases at longer time scales due to the prolonged reduction in
331 precipitation. At 36 months, it reaches trends between -0.03 and -0.04 (z-score) per decade for SPI, SPEI,
332 and SSI (Figure 5). For “Sur,” the behavior is similar, decreasing at longer scales and having between -0.016
333 and -0.025 per decade for SPI, SPEI, and SSI. On the other hand, all macrozones show an increase in the
334 trend in all the drought indices, with “Norte Grande” having the highest at 36 months (0.042 per decade).
335 Because of this, the SPEI (which uses AED) reached its lowest value in “Norte Grande,” with -0.03 at 36
336 months. Despite the other macrozones, “Austral” showed an increase in all indices, being the highest for
337 EDDI at 36 months (0.025) and the lowest for SSI, which shows only a minor increase in the trend (Figure 5
338 and Figure 4).

339 4.4. Impact for water supply and demand, and soil moisture in vegetation productivity

340 According to what is shown in Figure 6, Figure 7, and Table 4, forest seems to be the most resistant type
341 to drought. Showing that only “Centro” is slightly ($rsq = 0.25$) impacted by a 12-month soil moisture deficit
342 (SSI-12). In the “Norte Chico” and to a lesser extent in the “Norte Grande,” it is evident that a SSI-12 with
343 a $rsq = 0.45$ and a decrease in water supply (SPI-36 and SPEI-24 with $rsq = 0.28$ and 0.34, respectively)
344 have an impact on grasslands. However, this type was unaffected by soil moisture, water supply, or demand
345 in macrozones further south. The types that show to be most affected by variation in climate conditions
346 are shrublands, savannas, and croplands. For savannas in “Norte Chico,” the SSI-12 and SPI-24 reached
347 an rsq of 0.74 and 0.58, respectively. This value decreases to the south, but the SSI-12 is still the variable
348 explaining more of the variation in vegetation productivity ($rsq = 0.45$ in “Centro” and 0.2 in “Sur”). In
349 the case of croplands, the SPEI-12, SPI-36, and SSI-12 explain between 45% and 66% of “Norte Chico.”
350 The type of land most impacted by climatic variation was shrubland, where soil moisture explained 59%
351 and precipitation, 37%, in “Norte Chico” and “Centro,” with SSI-12 being the most relevant variable, then
352 SPI-36 in “Norte Chico” and SPI-24 in “Sur.”

353 5. Discussion

354 5.1. Drought trend and attribution to LULCC

355 ?, in a study at the global scale of drought trends, indicates that there have not been significant trends in
356 meteorological drought since 1950. Also, state that the increase in hydrological trend in some parts of the
357 globe (northeast Brazil and the Mediterranean region) is related to changes in land cover and specifically
358 to the rapidly increasing irrigated area, which consequently increases water extraction. [Kogan et al. \(2020\)](#)

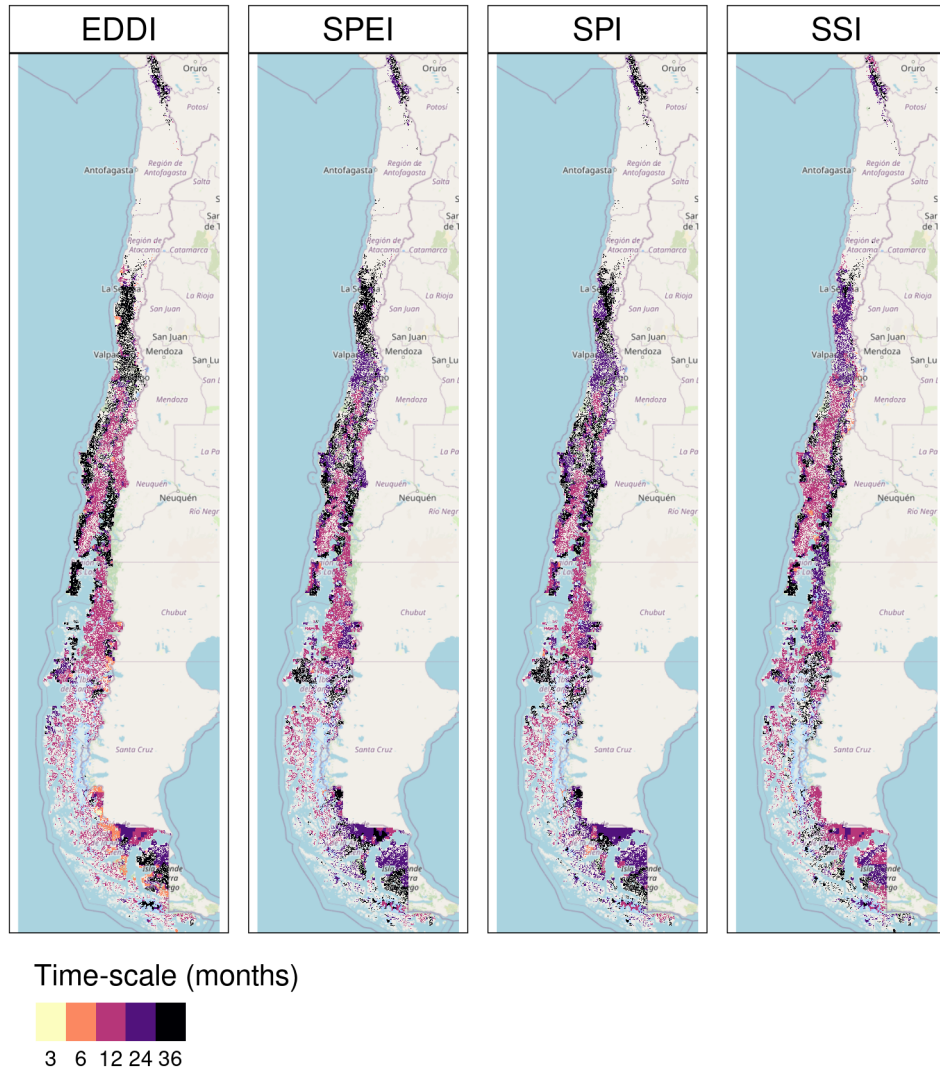


Figure 6: Time scales per drought index that reach the maximum coefficient of determination

359 analyzed the agricultural drought impact globally and in the main grain producer countries, finding that
 360 “since 1980, the Earth warming has not changed the drought area or intensity”.

361 In our study, we considered the variation in vegetation productivity in Chile for areas without changes
 362 in land cover macroclasses (see Section 4.2.2), to avoid misleading conclusions that could be related to the
 363 increase in water demand due to LULCC. Our results show a contrasting perspective. There has been
 364 a significant trend in the decline of vegetation productivity (zcNDVI) since 2000 for “Norte Chico” and
 365 “Centro,” which has been extreme between 2020 and 2022, seemingly due to an intense hydrological drought
 366 due to the persistence of the Mega Drought (Garreaud et al., 2017). Despite using the persistence mask
 367 for vegetation’s trend analysis, cropland, which is the most water-demand type, showed a decrease trend in
 368 “Norte Chico” and “Centro.” Also, there was an increase in barren land for both types. These changes are
 369 associated with a decrease in water demand from vegetation. Nonetheless, we used the persistent land cover
 370 to ensure that the pixel has the same class; in the case of croplands, it could happen that some areas had
 371 changed crops for others with higher water consumption. But this effect should be minor compared to the
 372 results from landcover macroclasses.

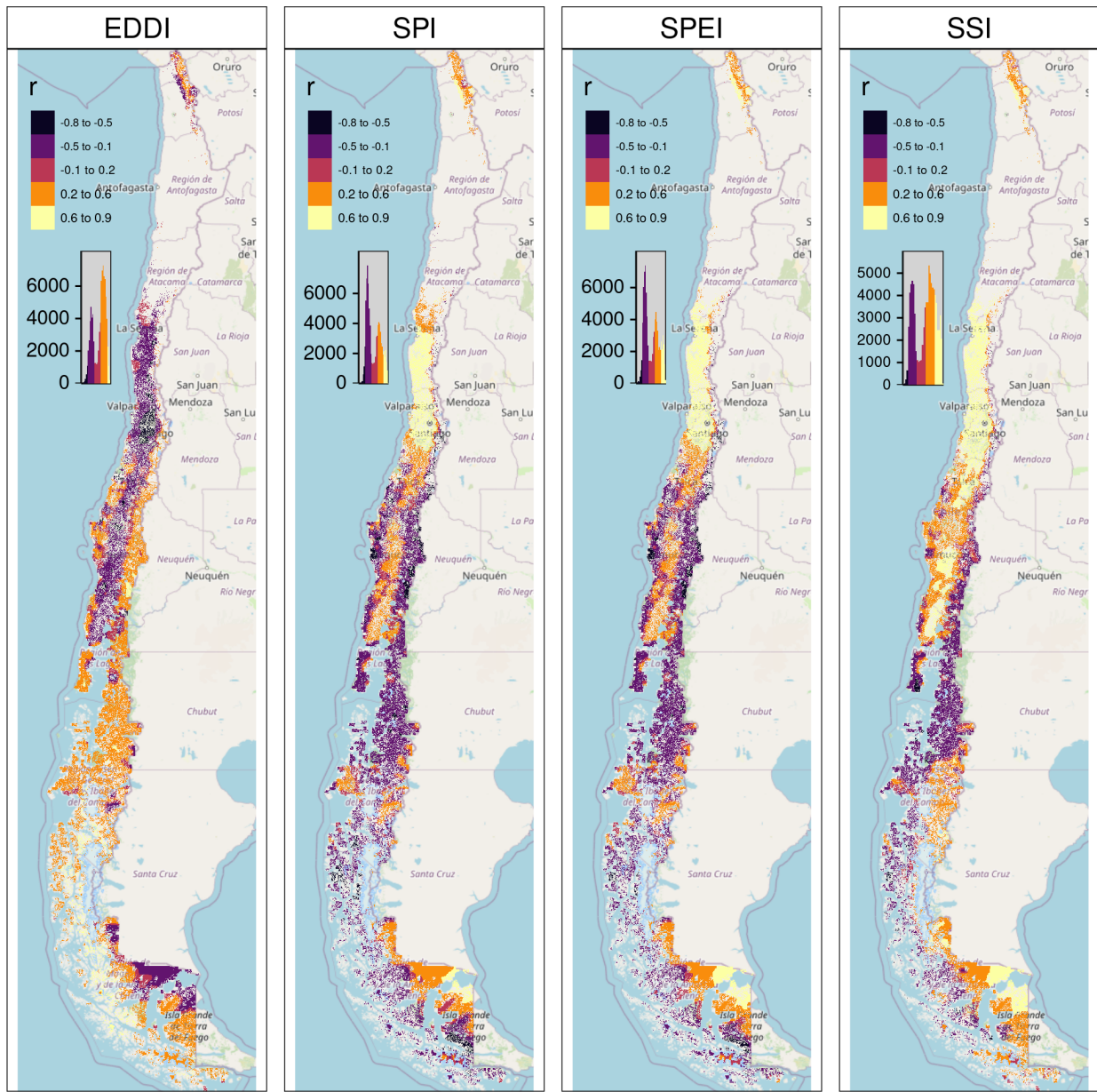


Figure 7: Pearson correlation value for the time scales and drought index that reach the maximum coefficient of determination

On the other hand, for “Norte Chico” and “Centro,” our results show a decrease in trends of water supply (SPI and SSI), which are higher at larger time scales and consequently impact the hydrological system. We claim that what occurred in central Chile defies findings made at the global level (?Kogan et al., 2020), demonstrating that a constant decrease in water supply rather than an increase in water demand (i.e., irrigated crops) is the main cause of the hydrological drought. Finally, central Chile has shown a diminishment in vegetation productivity for all macroclasses, mainly attributed to variation in water supply, i.e., precipitation, which could be strengthened by an increase in water demand by, for example, an increase in the surface area of irrigated crops.

381 5.2. Land cover types and their impact by drought

382 We found that shrubland, savannas (Chilean matorral), and croplands are the most sensitive to climate
383 conditions. Being most affected by the 12-month soil moisture deficit. In a study in the Yangtze River
384 Basin in China, Jiang2020 analyzed the impact of drought on vegetation using the SPEI and the Enhanced
385 Vegetation Index (EVI). They found that cropland was more sensitive to drought than cropland, showing
386 that cropland responds strongly to short- and medium-term drought (< SPEI-6). In our case, the SPEI-12
387 was the one that most impacted the croplands in “Norte Chico” and “Centro.” In general, most studies show
388 that croplands are most sensitive to short-term drought (< SPI-6) (Zambrano et al., 2016; Potopová et al.,
389 2015; Dai et al., 2020; Rhee et al., 2010). Short-term precipitation deficits impact soil water, and thus less
390 water is available for plant growth. However, we found that in “Norte Chico,” an SPI-36 and SPEI-12 had a
391 higher impact, which are associated with hydrological drought (long-term), and in “Centro,” an SPI-12 and
392 SPEI-12. Thus, we attribute this impact to the hydrological drought that has decreased groundwater storage
393 (Taucare et al., 2024), which in turn is impacted by long-term deficits, and consequently, the vegetation is
394 more dependent on groundwater. In “Sur” and “Austral,” the correlations between drought indices and
395 vegetation productivity decrease, as do the time scales that reach the maximum r-squared (4). What can
396 be explained is that, south of “Centro,” predominate forest and grassland, the most resistant types. Also,
397 drought episodes have been less frequent and intense. The drought episodes have had a lower impact on
398 water availability for vegetation.

399 Extreme drought conditions are an important driver of tree mortality, as shown by Senf et al. (2020) in
400 Europe. However, we found that forest is the type of land cover macroclass less affected by variation in
401 drought indices, being the most resistant land cover class to drought. Supporting this is Fathi-Taperasht
402 et al. (2022), who asserts that Indian forests are the most drought-resistant and recover rapidly. Similarly,
403 the work of Wu et al. (2024), who analyzed vegetation loss and recovery in response to meteorological
404 drought in the humid subtropical Pearl River basin in China, indicates that forests showed higher drought
405 resistance. Using Vegetation Optical Depth (VOD), kNDVI, and EVI, Xiao et al. (2023), tests the resistance
406 of ecosystems and finds that ecosystems with more forests are better able to handle severe droughts than
407 croplands. They attribute the difference to a deeper rooting depth of trees, a higher water storage capacity,
408 and different water use strategies between forest and cropland (Xiao et al., 2023).

409 In contrast to what we obtained, Venegas-González et al. (2023), who studied *Cryptocarya alba* and
410 *Beilschmiedia miersii* (both from the Lauraceae family) that live in sclerophyllous forests in Chile, found
411 that the trees’ overall growth had slowed down. This could mean that the natural dynamics of their forests
412 have changed. They attributed it to the cumulative effects of the unprecedented drought (i.e., hydrological
413 drought). Thus, we attribute that forest to being the most resistant to drought, due to the fact that most
414 of the species comprising it are highly resilient to water scarcity compared to the other land cover classes.
415 Nonetheless, if we want to go deep in our analysis, we should use earth observation data that is able to
416 capture a higher level of detail. For example, when we used MOD13A3 with a 1km spatial resolution to
417 measure vegetation condition, it took the average condition of 1 square kilometer. Then, to study how a type
418 of forest (e.g., sclerophyllous forest) changes in response to drought on a local level using remote sensing,
419 we should use operational products with higher spatial resolutions, such as those from Landsat or Sentinel.

420 5.3. Soil moisture, vegetation productivity, and agricultural drought.

421 The main external factors that affect biomass production by vegetation are ET and SM, and the rate
422 of ET in turn depends on the availability of water storage in the root zone. Thus, soil moisture plays a
423 key role in land carbon uptake and, consequently, in the production of biomass (Humphrey et al., 2021).
424 Moreover, Zhang et al. (2022) indicates there is a bidirectional causality between soil moisture and vegetation
425 productivity. Lastly, some studies have redefined agricultural drought as soil moisture drought from an
426 hydrological perspective (Van Loon et al., 2016; Samaniego et al., 2018). Even though soil moisture is the
427 external factor most determinant of vegetation biomass, there are multiple internal factors, such as species,
428 physiological characteristics, and plant hydraulics, that would affect vegetation productivity. Because of
429 that, we believe that agricultural drought, referring to the drought that impacts vegetation productivity, is
430 the most proper term, as originally defined by Wilhite and Glantz (1985).

431 The study results showed that the soil moisture-based drought index (SSI) was better at explaining vegetation productivity across land cover macroclasses than meteorological drought indices like SPI, SPEI, and EDDI. In the early growing season and especially in irrigated rather than rainfed croplands, soil moisture has better skills than SPI and SPEI for estimating gross primary production (GPP), according to Chatterjee et al. (2022)'s evaluation of the SPI and SPEI and their correlation with GPP in the CONUS. Also, Zhou et al. (2021) indicates that the monthly scaled Standardized Water Deficit Index (SWDI) can accurately show the effects of agricultural drought in most of China. Complementary, Nicolai-Shaw et al. (2017) analyzed the time-lag between SWDI and the Vegetation Condition Index (VCI), and they state that there was no or little time-lag with croplands but a significant time-lag in the case of forests.

440 In our case, there is strong spatial variability throughout Chile and between classes, mainly attributable to climate heterogeneity, hydrological status, or vegetation resistance to water scarcity. The semi-arid "Norte Chico" and the Mediterranean "Centro" were where SSI had the best performance. In Chile, medium-term deficits of 12 months are more relevant in the response of vegetation, which decreases to the south, and in the case of croplands, they seem to react in a shorter time, with six months (SSI-6) in "Centro." This variation for croplands could be related to the fact that in "Norte Chico," the majority of crops are irrigated, but to the south there is a higher proportion of rainfed agriculture, which is most dependent on the short-term availability of water. Rather, in the "Norte Chico," the orchards are more dependent on the storage of water in dams of groundwater reservoirs, which are affected by long-term drought (e.g., SPI-36).

449 5.4. Early drought forecasting for vegetation productivity

450 We analyzed the correlation between meteorological and soil moisture drought indices with zcNDVI. From 451 our findings, we could further use the drought indices and time scales that have the highest r-squared to 452 develop a combined model to forecast vegetation productivity in Chile. Despite the fact that SSI was the 453 best-performing index, the rest of the indices should help to enhance predictability. Zambrano et al. (2018) 454 proposed a prediction model for cropland surface in Chile at administrative units with a 1- to 6-month lead 455 time using zcNDVI from MODIS and climate oscillation indices. The results given were r-squared, ranging 456 from 0.95 at a 1-month lead time to 0.37 at a 6-month lead time. Thus, incorporating the results of this 457 study with those made by Zambrano et al. (2018), we could develop a combined forecasting model at the 458 pixel level for the macroclasses in Chile based on drought indices of water demand and supply and soil 459 moisture.

460 5.5. Future outlook (to complete)

461 6. Conclusion

462 There is a trend toward decreasing water supply in most parts of Chile, less in the "Austral," which is 463 stronger in the "Centro" and "Norte Chico." The whole country showed an increase in water demand. Vegetation 464 productivity only showed a decrease in the "Norte Chico" and "Centro," being highest for shrubland 465 and croplands. Forest is the land cover most resistant to drought, and shrubland and cropland are the most 466 sensitive.

467 A soil moisture deficit of 12 months (SSI-12) is highly correlated with vegetation productivity for the land 468 cover classes of shrubland, savannas, croplands, and forest in "Norte Chico" and "Centro." For the southern 469 part of the country with humid conditions, the correlation with SSI decreases. Soil moisture overcomes 470 the capacity to explain vegetation productivity over the supply and demand drought indices in the entire 471 territory.

472 The variation in vegetation productivity appears to be associated with climate variation rather than 473 anthropogenic factors (e.g., an increase in water demand by irrigated crops). Even though switching to more 474 demanding crops on the land could increase the impact of drought on vegetation, this would need to be 475 more thoroughly investigated, for instance at the watershed level.

476 The results of this study could help in the development of a robust forecasting system for land cover classes 477 in Chile., helping to improve preparedness for climate change impacts on vegetation.

478 **Supplementary material**479 **References**

- 480 Abramowitz, M., Stegun, I.A., 1968. Handbook of mathematical functions with formulas, graphs, and mathematical tables. volume 55. US Government printing office.
- 481 Aceituno, P., Boisier, J.P., Garreaud, R., Rondanelli, R., Ruttant, J.A., 2021. Climate and Weather in Chile, in: Fernández, B., Gironás, J. (Eds.), Water Resources of Chile. Springer International Publishing, Cham. volume 8, pp. 7–29. URL: http://link.springer.com/10.1007/978-3-030-56901-3_2.
- 482 AghaKouchak, A., 2014. A baseline probabilistic drought forecasting framework using standardized soil moisture index: application to the 2012 United States drought. *Hydrology and Earth System Sciences* 18, 2485–2492. URL: <https://hess.copernicus.org/articles/18/2485/2014/>, doi:10.5194/hess-18-2485-2014.
- 483 AghaKouchak, A., Mirchi, A., Madani, K., Di Baldassarre, G., Nazemi, A., Alborzi, A., Anjileli, H., Azarderakhsh, M., Chiang, F., Hassanzadeh, E., Huning, L.S., Mallakpour, I., Martinez, A., Mazdiyasni, O., Moftakhari, H., Norouzi, H., Sadegh, M., Sadeqi, D., Van Loon, A.F., Wanders, N., 2021. Anthropogenic Drought: Definition, Challenges, and Opportunities. *Reviews of Geophysics* 59, e2019RG000683. URL: <https://agupubs.onlinelibrary.wiley.com/doi/10.1029/2019RG000683>, doi:10.1029/2019RG000683.
- 484 Akinyemi, F.O., 2021. Vegetation Trends, Drought Severity and Land Use-Land Cover Change during the Growing Season in Semi-Arid Contexts. *Remote Sensing* 2021, Vol. 13, Page 836 13, 836. URL: <https://www.mdpi.com/2072-4292/13/5/836/htm>, doi:10.3390/RS13050836. publisher: Multidisciplinary Digital Publishing Institute.
- 485 Bakker, K., 2012. Water Security: Research Challenges and Opportunities. *Science* 337, 914–915. URL: <https://www.science.org/doi/10.1126/science.1226337>, doi:10.1126/science.1226337.
- 486 Beck, H.E., McVicar, T.R., Vergopolan, N., Berg, A., Lutsko, N.J., Dufour, A., Zeng, Z., Jiang, X., van Dijk, A.I.J.M., Miralles, D.G., 2023. High-resolution (1 km) Köppen-Geiger maps for 1901–2099 based on constrained CMIP6 projections. *Scientific Data* 10. URL: <http://dx.doi.org/10.1038/s41597-023-02549-6>, doi:10.1038/s41597-023-02549-6.
- 487 Beguería, S., Vicente-Serrano, S.M., 2023. SPEI: Calculation of the Standardized Precipitation-Evapotranspiration Index. URL: <https://CRAN.R-project.org/package=SPEI>.
- 488 Boisier, J.P., Alvarez-Garreton, C., Cordero, R.R., Damiani, A., Gallardo, L., Garreaud, R.D., Lambert, F., Ramallo, C., Rojas, M., Rondanelli, R., 2018. Anthropogenic drying in central-southern Chile evidenced by long-term observations and climate model simulations. *Elementa* 6, 74. URL: <https://www.elementascience.org/article/10.1525/elementa.328/>, doi:10.1525/elementa.328.
- 489 Calvin, K., Dasgupta, D., Krinner, G., Mukherji, A., Thorne, P.W., Trisos, C., Romero, J., Aldunce, P., Barrett, K., Blanco, G., Cheung, W.W., Connors, S., Denton, F., Diongue-Niang, A., Dodman, D., Garschagen, M., Geden, O., Hayward, B., Jones, C., Jotzo, F., Krug, T., Lasco, R., Lee, Y.Y., Masson-Delmotte, V., Meinshausen, M., Mintenbeck, K., Mokssit, A., Otto, F.E., Pathak, M., Pirani, A., Poloczanska, E., Pörtner, H.O., Revi, A., Roberts, D.C., Roy, J., Ruane, A.C., Skea, J., Shukla, P.R., Slade, R., Slangen, A., Sokona, Y., Sörensson, A.A., Tignor, M., Van Vuuren, D., Wei, Y.M., Winkler, H., Zhai, P., Zommers, Z., Hourcade, J.C., Johnson, F.X., Pachauri, S., Simpson, N.P., Singh, C., Thomas, A., Totin, E., Arias, P., Bustamante, M., Elgizouli, I., Flato, G., Howden, M., Méndez-Vallejo, C., Pereira, J.J., Pichs-Madruga, R., Rose, S.K., Saheb, Y., Sánchez Rodríguez, R., Ürge Vorsatz, D., Xiao, C., Yassa, N., Alegria, A., Armour, K., Bednar-Friedl, B., Blok, K., Cissé, G., Dentener, F., Eriksen, S., Fischer, E., Garner, G., Guiavarch, C., Haasnoot, M., Hansen, G., Hauser, M., Hawkins, E., Hermans, T., Kopp, R., Leprince-Ringuet, N., Lewis, J., Ley, D., Ludden, C., Niamir, L., Nicholls, Z., Some, S., Szopa, S., Trewin, B., Van Der Wijst, K.I., Winter, G., Witting, M., Birt, A., Ha, M., Romero, J., Kim, J., Haites, E.F., Jung, Y., Stavins, R., Birt, A., Ha, M., Orendain, D.J.A., Ignon, L., Park, S., Park, Y., Reisinger, A., Cammaramo, D., Fischlin, A., Fuglestvedt, J.S., Hansen, G., Ludden, C., Masson-Delmotte, V., Matthews, J.R., Mintenbeck, K., Pirani, A., Poloczanska, E., Leprince-Ringuet, N., Péan, C., 2023. IPCC, 2023: Climate Change 2023: Synthesis Report. Contribution of Working Groups I, II and III to the Sixth Assessment Report of the Intergovernmental Panel on Climate Change [Core Writing Team, H. Lee and J. Romero (eds.)]. IPCC, Geneva, Switzerland. Technical Report. Intergovernmental Panel on Climate Change (IPCC). URL: <https://www.ipcc.ch/report/ar6/syr/>.
- 490 Chamling, M., Bera, B., 2020. Spatio-temporal Patterns of Land Use/Land Cover Change in the Bhutan–Bengal Foothill Region Between 1987 and 2019: Study Towards Geospatial Applications and Policy Making. *Earth Systems and Environment* 4, 117–130. URL: <http://link.springer.com/10.1007/s41748-020-00150-0>, doi:10.1007/s41748-020-00150-0.
- 491 Chatterjee, S., Desai, A.R., Zhu, J., Townsend, P.A., Huang, J., 2022. Soil moisture as an essential component for delineating and forecasting agricultural rather than meteorological drought. *Remote Sensing of Environment* 269, 112833. URL: <https://linkinghub.elsevier.com/retrieve/pii/S0034425721005538>, doi:10.1016/j.rse.2021.112833.
- 492 Chen, J., Shao, Z., Huang, X., Zhuang, Q., Dang, C., Cai, B., Zheng, X., Ding, Q., 2022. Assessing the impact of drought-land cover change on global vegetation greenness and productivity. *Science of The Total Environment* 852, 158499. URL: <https://linkinghub.elsevier.com/retrieve/pii/S004896972205598X>, doi:10.1016/j.scitotenv.2022.158499.
- 493 Crausbay, S.D., Ramirez, A.R., Carter, S.L., Cross, M.S., Hall, K.R., Bathke, D.J., Betancourt, J.L., Colt, S., Cravens, A.E., Dalton, M.S., Dunham, J.B., Hay, L.E., Hayes, M.J., McEvoy, J., McNutt, C.A., Moritz, M.A., Nislow, K.H., Raheem, N., Sanford, T., 2017. Defining Ecological Drought for the Twenty-First Century. *Bulletin of the American Meteorological Society* 98, 2543–2550. URL: <https://journals.ametsoc.org/view/journals/bams/98/12/bams-d-16-0292.1.xml>, doi:10.1175/BAMS-D-16-0292.1. publisher: American Meteorological Society.
- 494 Dai, M., Huang, S., Huang, Q., Leng, G., Guo, Y., Wang, L., Fang, W., Li, P., Zheng, X., 2020. Assessing agricultural drought risk and its dynamic evolution characteristics. *Agricultural Water Management* 231, 106003. URL: <https://linkinghub.elsevier.com/retrieve/pii/S0378377419316531>, doi:10.1016/j.agwat.2020.106003.

- 541 Didan, K., 2015. MOD13Q1 MODIS/Terra Vegetation Indices 16-Day L3 Global 250m SIN Grid V006. Technical Report.
 542 NASA EOSDIS Land Processes DAAC. doi:<http://dx.doi.org/10.5067/MODIS/MOD13Q1.006>.
- 543 Fathi-Taperasht, A., Shafizadeh-Moghadam, H., Minaei, M., Xu, T., 2022. Influence of drought duration and severity on
 544 drought recovery period for different land cover types: evaluation using MODIS-based indices. Ecological Indicators 141,
 545 109146. URL: <https://linkinghub.elsevier.com/retrieve/pii/S1470160X22006185>, doi:[10.1016/j.ecolind.2022.109146](https://doi.org/10.1016/j.ecolind.2022.109146).
- 546 Friedl, M., Sulla-Menashe, D., 2019. MCD12Q1 MODIS/Terra+Aqua Land Cover Type Yearly L3 Global 500m SIN Grid V006
 547 [Data set]. NASA EOSDIS Land Processes DAAC. doi:[10.5067/MODIS/MCD12Q1.006](https://doi.org/10.5067/MODIS/MCD12Q1.006).
- 548 Fuentes, I., Fuster, R., Avilés, D., Vervoort, W., 2021. Water scarcity in central Chile: the effect of climate and land cover
 549 changes on hydrologic resources. Hydrological Sciences Journal 66, 1028–1044. URL: <https://www.tandfonline.com/doi/full/10.1080/02626667.2021.1903475>, doi:[10.1080/02626667.2021.1903475](https://doi.org/10.1080/02626667.2021.1903475).
- 550 Garreaud, R., Alvarez-Garreton, C., Barichivich, J., Boisier, J.P., Christie, D., Galleguillos, M., LeQuenne, C., McPhee, J.,
 551 Zambrano-Bigiarini, M., 2017. The 2010–2015 mega drought in Central Chile: Impacts on regional hydroclimate and
 552 vegetation. Hydrology and Earth System Sciences Discussions 2017, 1–37. URL: <http://www.hydrol-earth-syst-sci-discuss.net/hess-2017-191/>, doi:[10.5194/hess-2017-191](https://doi.org/10.5194/hess-2017-191).
- 553 Garreaud, R.D., 2009. The Andes climate and weather. Advances in Geosciences 22, 3–11. URL: <https://adgeo.copernicus.org/articles/22/3/2009/>, doi:[10.5194/adgeo-22-3-2009](https://doi.org/10.5194/adgeo-22-3-2009).
- 554 Garreaud, R.D., Boisier, J.P., Rondanelli, R., Montecinos, A., Sepúlveda, H.H., Veloso-Aguila, D., 2020. The Central Chile
 555 Mega Drought (2010–2018): A climate dynamics perspective. International Journal of Climatology 40, 421–439. URL:
 556 <https://rmets.onlinelibrary.wiley.com/doi/10.1002/joc.6219>, doi:[10.1002/joc.6219](https://doi.org/10.1002/joc.6219).
- 557 Hao, Z., AghaKouchak, A., 2013. Multivariate Standardized Drought Index: A parametric multi-index model. Advances in Wa-
 558 ter Resources 57, 12–18. URL: <https://linkinghub.elsevier.com/retrieve/pii/S0309170813000493>, doi:[10.1016/j.advwatres.2013.03.009](https://doi.org/10.1016/j.advwatres.2013.03.009).
- 559 Hargreaves, G.H., 1994. Defining and Using Reference Evapotranspiration. Journal of Irrigation and Drainage Engineering 120,
 560 1132–1139. URL: [https://ascelibrary.org/doi/10.1061/\(ASCE\)0733-9437\(1994\)120:6\(1132\)](https://ascelibrary.org/doi/10.1061/(ASCE)0733-9437(1994)120:6(1132)), doi:[10.1061/\(ASCE\)0733-9437\(1994\)120:6\(1132\)](https://doi.org/10.1061/(ASCE)0733-9437(1994)120:6(1132)).
- 561 Hargreaves, G.H., Samani, Z.A., 1985. Reference crop evapotranspiration from temperature. Applied engineering in agriculture
 562 1, 96–99.
- 563 Hijmans, R.J., 2023. terra: Spatial Data Analysis. URL: <https://CRAN.R-project.org/package=terra>.
- 564 Ho, T.K., 1995. Random decision forests, in: Proceedings of 3rd international conference on document analysis and recognition,
 565 IEEE. pp. 278–282.
- 566 Hobbins, M.T., Wood, A., McEvoy, D.J., Huntington, J.L., Morton, C., Anderson, M., Hain, C., 2016. The Evaporative Demand
 567 Drought Index. Part I: Linking Drought Evolution to Variations in Evaporative Demand. Journal of Hydrometeorology 17,
 568 1745–1761. URL: <http://journals.ametsoc.org/doi/10.1175/JHM-D-15-0121.1>, doi:[10.1175/JHM-D-15-0121.1](https://doi.org/10.1175/JHM-D-15-0121.1).
- 569 Hoerl, A.E., Kennard, R.W., 1970. Ridge Regression: Biased Estimation for Nonorthogonal Problems. Technometrics 12, 55–67.
 570 URL: <https://www.tandfonline.com/doi/abs/10.1080/00401706.1970.10488634>, doi:[10.1080/00401706.1970.10488634](https://doi.org/10.1080/00401706.1970.10488634).
- 571 Homer, C., Dewitz, J., Jin, S., Xian, G., Costello, C., Danielson, P., Gass, L., Funk, M., Wickham, J., Stehman, S., Auch, R.,
 572 Riitters, K., 2020. Conterminous United States land cover change patterns 2001–2016 from the 2016 National Land Cover
 573 Database. ISPRS Journal of Photogrammetry and Remote Sensing 162, 184–199. URL: <https://linkinghub.elsevier.com/retrieve/pii/S0924271620300587>, doi:[10.1016/j.isprsjprs.2020.02.019](https://doi.org/10.1016/j.isprsjprs.2020.02.019).
- 574 Hufkens, K., Stauffer, R., Campitelli, E., 2019. The ecwmfr package: an interface to ECMWF API endpoints. URL: <https://bluegreen-labs.github.io/ecmwfr/>.
- 575 Humphrey, V., Berg, A., Ciais, P., Gentine, P., Jung, M., Reichstein, M., Seneviratne, S.I., Frankenberg, C., 2021. Soil
 576 moisture–atmosphere feedback dominates land carbon uptake variability. Nature 592, 65–69. URL: <https://www.nature.com/articles/s41586-021-03325-5>, doi:[10.1038/s41586-021-03325-5](https://doi.org/10.1038/s41586-021-03325-5).
- 577 IPCC, 2013. Climate Change 2013: The Physical Science Basis. Contribution of Working Group I to the Fifth Assessment
 578 Report of the Intergovernmental Panel on Climate Change. Cambridge University Press, Cambridge, UK; New York, USA.
 579 URL: www.climatechange2013.org, doi:[10.1017/CBO9781107415324](https://doi.org/10.1017/CBO9781107415324).
- 580 Kendall, M., 1975. Rank correlation methods (4th ed. 2d impression). Griffin.
- 581 Kogan, F., Guo, W., Yang, W., 2020. Near 40-year drought trend during 1981–2019 earth warming and food security. Geomatics,
 582 Natural Hazards and Risk 11, 469–490. URL: <https://www.tandfonline.com/doi/full/10.1080/19475705.2020.1730452>, doi:[10.1080/19475705.2020.1730452](https://doi.org/10.1080/19475705.2020.1730452).
- 583 Luebert, F., Pliscott, P., 2022. The vegetation of Chile and the EcoVeg approach in the context of the International Vegetation
 584 Classification project. Vegetation Classification and Survey 3, 15–28. URL: <https://vcs.pensoft.net/article/67893/>, doi:[10.3897/VCS.67893](https://doi.org/10.3897/VCS.67893).
- 585 Luyssaert, S., Jammet, M., Stoy, P.C., Estel, S., Pongratz, J., Ceschia, E., Churkina, G., Don, A., Erb, K., Ferlicoq, M.,
 586 Gielen, B., Grünwald, T., Houghton, R.A., Klumpp, K., Knohl, A., Kolb, T., Kuemmerle, T., Laurila, T., Lohila, A.,
 587 Loustau, D., McGrath, M.J., Meyfroidt, P., Moors, E.J., Naudts, K., Novick, K., Otto, J., Pilegaard, K., Pio, C.A., Rambal,
 588 S., Rebmann, C., Ryder, J., Suyker, A.E., Varlagin, A., Wattenbach, M., Dolman, A.J., 2014. Land management and
 589 land-cover change have impacts of similar magnitude on surface temperature. Nature Climate Change 4, 389–393. URL:
 590 <https://www.nature.com/articles/nclimate2196>, doi:[10.1038/nclimate2196](https://doi.org/10.1038/nclimate2196).
- 591 Masson-Delmotte, V., P.Z.A.P.S.L.C.C.P.S.B.N.C.Y.C.L.G.M.I.G.M.H.K.L.E.L.J.B.R.M.T.K.M.T.W.O.Y.R.Y.a.B.Z.e., 2021.
 592 IPCC, 2021: Climate Change 2021: The Physical Science Basis. Contribution of Working Group I to the Sixth Assessment
 593 Report of the Intergovernmental Panel on Climate Change. Technical Report. URL: <https://www.ipcc.ch/>. publication
 594 Title: Cambridge University Press. In Press.
- 595 McEvoy, D.J., Huntington, J.L., Hobbins, M.T., Wood, A., Morton, C., Anderson, M., Hain, C., 2016. The Evaporative Demand
 596

- 606 Drought Index. Part II: CONUS-Wide Assessment against Common Drought Indicators. *Journal of Hydrometeorology* 17,
 607 1763–1779. URL: <http://journals.ametsoc.org/doi/10.1175/JHM-D-15-0122.1>, doi:[10.1175/JHM-D-15-0122.1](https://doi.org/10.1175/JHM-D-15-0122.1).
- 608 McKee, T.B., Doesken, N.J., Kleist, J., 1993. The relationship of drought frequency and duration to time scales. In: Proceedings
 609 of the Ninth Conference on Applied Climatology. American Meteorological Society , 179–184.
- 610 Meroni, M., Rembold, F., Fasbender, D., Vrieling, A., 2017. Evaluation of the Standardized Precipitation Index as an early
 611 predictor of seasonal vegetation production anomalies in the Sahel. *Remote Sensing Letters* 8, 301–310. URL: <https://www.tandfonline.com/doi/full/10.1080/2150704X.2016.1264020>, doi:[10.1080/2150704X.2016.1264020](https://doi.org/10.1080/2150704X.2016.1264020).
- 612 Miranda, A., Lara, A., Altamirano, A., Di Bella, C., González, M.E., Julio Camarero, J., 2020. Forest browning trends in
 613 response to drought in a highly threatened mediterranean landscape of South America. *Ecological Indicators* 115, 106401.
 614 URL: <https://linkinghub.elsevier.com/retrieve/pii/S1470160X20303381>, doi:[10.1016/j.ecolind.2020.106401](https://doi.org/10.1016/j.ecolind.2020.106401).
- 615 Miranda, A., Syphard, A.D., Berdugo, M., Carrasco, J., Gómez-González, S., Ovalle, J.F., Delpiano, C.A., Vargas, S.,
 616 Squeo, F.A., Miranda, M.D., Dobbs, C., Mentler, R., Lara, A., Garreaud, R., 2023. Widespread synchronous decline
 617 of Mediterranean-type forest driven by accelerated aridity. *Nature Plants* 9, 1810–1817. URL: <https://www.nature.com/articles/s41477-023-01541-7>, doi:[10.1038/s41477-023-01541-7](https://doi.org/10.1038/s41477-023-01541-7).
- 618 Muñoz-Sabater, J., Dutra, E., Agustí-Panareda, A., Albergel, C., Arduini, G., Balsamo, G., Boussetta, S., Choulga, M.,
 619 Harrigan, S., Hersbach, H., Martens, B., Miralles, D.G., Piles, M., Rodríguez-Fernández, N.J., Zsoter, E., Buontempo, C.,
 620 Thépaut, J.N., 2021. ERA5-Land: a state-of-the-art global reanalysis dataset for land applications. *Earth System Science
 621 Data* 13, 4349–4383. URL: <https://essd.copernicus.org/articles/13/4349/2021/>, doi:[10.5194/essd-13-4349-2021](https://doi.org/10.5194/essd-13-4349-2021).
- 622 Nicolai-Shaw, N., Zschieschler, J., Hirschi, M., Gudmundsson, L., Seneviratne, S.I., 2017. A drought event composite analysis
 623 using satellite remote-sensing based soil moisture. *Remote Sensing of Environment* 203, 216–225. URL: <https://linkinghub.elsevier.com/retrieve/pii/S0034425717302729>, doi:[10.1016/j.rse.2017.06.014](https://doi.org/10.1016/j.rse.2017.06.014).
- 624 Pebesma, E., 2018. Simple Features for R: Standardized Support for Spatial Vector Data. *The R Journal* 10, 439–446. URL:
 625 <https://doi.org/10.32614/RJ-2018-009>, doi:[10.32614/RJ-2018-009](https://doi.org/10.32614/RJ-2018-009).
- 626 Pebesma, E., Bivand, R., 2023. Spatial Data Science: With applications in R. Chapman and Hall/CRC, London. URL:
 627 <https://r-spatial.org/book/>.
- 628 Peng, D., Zhang, B., Wu, C., Huete, A.R., Gonsamo, A., Lei, L., Ponce-Campos, G.E., Liu, X., Wu, Y., 2017. Country-level
 629 net primary production distribution and response to drought and land cover change. *Science of The Total Environment* 574,
 630 65–77. URL: <https://linkinghub.elsevier.com/retrieve/pii/S0048969716319507>, doi:[10.1016/j.scitotenv.2016.09.033](https://doi.org/10.1016/j.scitotenv.2016.09.033).
- 631 Pitman, A.J., De Noblet-Ducoudré, N., Avila, F.B., Alexander, L.V., Boisier, J.P., Brovkin, V., Delire, C., Cruz, F., Donat,
 632 M.G., Gayler, V., Van Den Hurk, B., Reick, C., Volodire, A., 2012. Effects of land cover change on temperature and
 633 rainfall extremes in multi-model ensemble simulations. *Earth System Dynamics* 3, 213–231. URL: <https://esd.copernicus.org/articles/3/213/2012/>, doi:[10.5194/esd-3-213-2012](https://doi.org/10.5194/esd-3-213-2012).
- 634 Potopová, V., Stepánek, P., Možný, M., Türkott, L., Soukup, J., 2015. Performance of the standarised precipitation evapotranspiration
 635 index at various lags for agricultural drought risk assessment in the {C}zech {R}epublic. *Agricultural and Forest
 636 Meteorology* 202, 26–38.
- 637 R Core Team, 2023. R: A Language and Environment for Statistical Computing. R Foundation for Statistical Computing,
 638 Vienna, Austria. URL: <https://www.R-project.org/>.
- 639 Rhee, J., Im, J., Carbone, G.J., 2010. Monitoring agricultural drought for arid and humid regions using multi-sensor remote
 640 sensing data. *Remote Sensing of Environment* 114, 2875–2887. URL: <http://www.sciencedirect.com/science/article/pii/S003442571000221X>, doi:[10.1016/j.rse.2010.07.005](https://doi.org/10.1016/j.rse.2010.07.005).
- 641 Samaniego, L., Thober, S., Kumar, R., Wanders, N., Rakovec, O., Pan, M., Zink, M., Sheffield, J., Wood, E.F., Marx, A.,
 642 2018. Anthropogenic warming exacerbates European soil moisture droughts. *Nature Climate Change* 8, 421–426. URL:
 643 <https://www.nature.com/articles/s41558-018-0138-5>, doi:[10.1038/s41558-018-0138-5](https://doi.org/10.1038/s41558-018-0138-5).
- 644 Sen, P.K., 1968. Estimates of the Regression Coefficient Based on Kendall's Tau. *Journal of the American Statistical Association*
 645 63, 1379–1389. URL: <http://www.tandfonline.com/doi/abs/10.1080/01621459.1968.10480934>, doi:[10.1080/01621459.1968.10480934](https://doi.org/10.1080/01621459.1968.10480934).
- 646 Senf, C., Buras, A., Zang, C.S., Rammig, A., Seidl, R., 2020. Excess forest mortality is consistently linked to drought
 647 across Europe. *Nature Communications* 11, 6200. URL: <https://www.nature.com/articles/s41467-020-19924-1>, doi:[10.1038/s41467-020-19924-1](https://doi.org/10.1038/s41467-020-19924-1).
- 648 Slette, I.J., Post, A.K., Awad, M., Even, T., Punzalan, A., Williams, S., Smith, M.D., Knapp, A.K., 2019. How ecologists
 649 define drought, and why we should do better. *Global Change Biology* 25, 3193–3200. URL: <https://onlinelibrary.wiley.com/doi/10.1111/gcb.14747>, doi:[10.1111/gcb.14747](https://doi.org/10.1111/gcb.14747).
- 650 Song, X.P., Hansen, M.C., Stehman, S.V., Potapov, P.V., Tyukavina, A., Vermote, E.F., Townshend, J.R., 2018. Global land
 651 change from 1982 to 2016. *Nature* 560, 639–643. URL: <https://www.nature.com/articles/s41586-018-0411-9>, doi:[10.1038/s41586-018-0411-9](https://doi.org/10.1038/s41586-018-0411-9).
- 652 Taucare, M., Viguier, B., Figueroa, R., Daniele, L., 2024. The alarming state of Central Chile's groundwater resources: A
 653 paradigmatic case of a lasting overexploitation. *Science of The Total Environment* 906, 167723. URL: <https://linkinghub.elsevier.com/retrieve/pii/S0048969723063507>, doi:[10.1016/j.scitotenv.2023.167723](https://doi.org/10.1016/j.scitotenv.2023.167723).
- 654 Tennekes, M., 2018. tmap: Thematic Maps in R. *Journal of Statistical Software* 84, 1–39. doi:[10.18637/jss.v084.i06](https://doi.org/10.18637/jss.v084.i06).
- 655 Tibshirani, R., Bien, J., Friedman, J., Hastie, T., Simon, N., Taylor, J., Tibshirani, R.J., 2010. Strong rules for discarding
 656 predictors in lasso-type problems. URL: <http://arxiv.org/abs/1011.2234>.
- 657 Urrutia-Jalabert, R., González, M.E., González-Reyes, A., Lara, A., Garreaud, R., 2018. Climate variability and forest fires in
 658 central and south-central Chile. *Ecosphere* 9, e02171. URL: <https://esajournals.onlinelibrary.wiley.com/doi/10.1002/ecs2.2171>, doi:[10.1002/ecs2.2171](https://doi.org/10.1002/ecs2.2171).
- 659 Van Loon, A.F., Gleeson, T., Clark, J., Van Dijk, A.I., Stahl, K., Hannaford, J., Di Baldassarre, G., Teuling, A.J., Tallaksen,
 660

- 671 L.M., Uijlenhoet, R., Hannah, D.M., Sheffield, J., Svoboda, M., Verbeiren, B., Wagener, T., Rangecroft, S., Wanders, N.,
 672 Van Lanen, H.A., 2016. Drought in the Anthropocene. *Nature Geoscience* 9, 89–91. doi:[10.1038/ngeo2646](https://doi.org/10.1038/ngeo2646).
 673 Venegas-González, A., Juñent, F.R., Gutiérrez, A.G., Filho, M.T., 2018. Recent radial growth decline in response to increased
 674 drought conditions in the northernmost Nothofagus populations from South America. *Forest Ecology and Management* 409,
 675 94–104. URL: <https://linkinghub.elsevier.com/retrieve/pii/S0378112717313993>, doi:[10.1016/j.foreco.2017.11.006](https://doi.org/10.1016/j.foreco.2017.11.006).
 676 Venegas-González, A., Muñoz, A.A., Carpintero-Gibson, S., González-Reyes, A., Schneider, I., Gipolou-Zuñiga, T., Aguilera-
 677 Betti, I., Roig, F.A., 2023. Sclerophyllous Forest Tree Growth Under the Influence of a Historic Megadrought in the
 678 Mediterranean Ecoregion of Chile. *Ecosystems* 26, 344–361. URL: <https://link.springer.com/10.1007/s10021-022-00760-x>,
 679 doi:[10.1007/s10021-022-00760-x](https://doi.org/10.1007/s10021-022-00760-x).
 680 Vicente-Serrano, S.M., Azorin-Molina, C., Sanchez-Lorenzo, A., Revuelto, J., López-Moreno, J.I., González-Hidalgo, J.C.,
 681 Moran-Tejeda, E., Espejo, F., 2014. Reference evapotranspiration variability and trends in Spain, 1961–2011. *Global
 682 and Planetary Change* 121, 26–40. URL: <https://linkinghub.elsevier.com/retrieve/pii/S0921818114001180>, doi:[10.1016/j.gloplacha.2014.06.005](https://doi.org/10.1016/j.gloplacha.2014.06.005).
 683 Vicente-Serrano, S.M., Miralles, D.G., Domínguez-Castro, F., Azorin-Molina, C., El Kenawy, A., McVicar, T.R., Tomás-
 684 Burguera, M., Beguería, S., Maneta, M., Peña-Gallardo, M., 2018. Global Assessment of the Standardized Evapotranspiration
 685 Deficit Index (SEDI) for Drought Analysis and Monitoring. *Journal of Climate* 31, 5371–5393. URL: <https://journals.ametsoc.org/doi/10.1175/JCLI-D-17-0775.1>, doi:[10.1175/JCLI-D-17-0775.1](https://doi.org/10.1175/JCLI-D-17-0775.1).
 686 Vicente-Serrano, S.M., Peña-Angulo, D., Beguería, S., Domínguez-Castro, F., Tomás-Burguera, M., Noguera, I., Gimeno-Sotelo,
 687 L., El Kenawy, A., 2022. Global drought trends and future projections. *Philosophical Transactions of the Royal Society A:
 688 Mathematical, Physical and Engineering Sciences* 380, 20210285. URL: <https://royalsocietypublishing.org/doi/10.1098/rsta.2021.0285>, doi:[10.1098/rsta.2021.0285](https://doi.org/10.1098/rsta.2021.0285).
 689 Wickham, H., Averick, M., Bryan, J., Chang, W., McGowan, L.D., François, R., Grolemund, G., Hayes, A., Henry, L., Hester,
 690 J., Kuhn, M., Pedersen, T.L., Miller, E., Bache, S.M., Müller, K., Ooms, J., Robinson, D., Seidel, D.P., Spinu, V., Takahashi,
 691 K., Vaughan, D., Wilke, C., Woo, K., Yutani, H., 2019. Welcome to the tidyverse. *Journal of Open Source Software* 4, 1686.
 692 doi:[10.21105/joss.01686](https://doi.org/10.21105/joss.01686).
 693 Wilhite, D.A., Glantz, M.H., 1985. Understanding: The drought phenomenon: The role of definitions. *Water International* 10,
 694 111–120. URL: <http://dx.doi.org/10.1080/02508068508686328>, doi:[10.1080/02508068508686328](https://doi.org/10.1080/02508068508686328).
 695 Wilks, D.S., 2011. Empirical distributions and exploratory data analysis. *Statistical Methods in the Atmospheric Sciences* 100.
 696 Winkler, K., Fuchs, R., Rounsevell, M., Herold, M., 2021. Global land use changes are four times greater than previously
 697 estimated. *Nature Communications* 12, 2501. URL: <https://www.nature.com/articles/s41467-021-22702-2>, doi:[10.1038/s41467-021-22702-2](https://doi.org/10.1038/s41467-021-22702-2).
 698 Wu, C., Zhong, L., Yeh, P.J.F., Gong, Z., Lv, W., Chen, B., Zhou, J., Li, J., Wang, S., 2024. An evaluation framework
 699 for quantifying vegetation loss and recovery in response to meteorological drought based on SPEI and NDVI. *Science of
 700 The Total Environment* 906, 167632. URL: <https://linkinghub.elsevier.com/retrieve/pii/S0048969723062599>, doi:[10.1016/j.scitotenv.2023.167632](https://doi.org/10.1016/j.scitotenv.2023.167632).
 701 Xiao, C., Zaehle, S., Yang, H., Wigneron, J.P., Schmullius, C., Bastos, A., 2023. Land cover and management effects on
 702 ecosystem resistance to drought stress. *Earth System Dynamics* 14, 1211–1237. URL: <https://esd.copernicus.org/articles/14/1211/2023/>, doi:[10.5194/esd-14-1211-2023](https://doi.org/10.5194/esd-14-1211-2023).
 703 Yang, J., Huang, X., 2021. The 30 m annual land cover dataset and its dynamics in China from 1990 to 2019. *Earth System
 704 Science Data* 13, 3907–3925. URL: <https://essd.copernicus.org/articles/13/3907/2021/>, doi:[10.5194/essd-13-3907-2021](https://doi.org/10.5194/essd-13-3907-2021).
 705 Zambrano, F., 2023. Four decades of satellite data for agricultural drought monitoring throughout the growing season in Central
 706 Chile, in: Vijay P. Singh Deepak Jhajharia, R.M., Kumar, R. (Eds.), *Integrated Drought Management*, Two Volume Set.
 707 CRC Press, p. 28.
 708 Zambrano, F., Lillo-Saavedra, M., Verbist, K., Lagos, O., 2016. Sixteen years of agricultural drought assessment of the
 709 biobío region in chile using a 250 m resolution vegetation condition index (VCI). *Remote Sensing* 8, 1–20. URL: <http://www.mdpi.com/2072-4292/8/6/530>, doi:[10.3390/rs8060530](https://doi.org/10.3390/rs8060530). publisher: Multidisciplinary Digital Publishing Institute.
 710 Zambrano, F., Vrielinck, A., Nelson, A., Meroni, M., Tadesse, T., 2018. Prediction of drought-induced reduction of agricultural
 711 productivity in Chile from MODIS, rainfall estimates, and climate oscillation indices. *Remote Sensing of Environment*
 712 219, 15–30. URL: <https://www.sciencedirect.com/science/article/pii/S0034425718304541>, doi:[10.1016/j.rse.2018.10.006](https://doi.org/10.1016/j.rse.2018.10.006).
 713 publisher: Elsevier.
 714 Zhang, W., Wei, F., Horion, S., Fensholt, R., Forkel, M., Brandt, M., 2022. Global quantification of the bidirectional de-
 715 pendency between soil moisture and vegetation productivity. *Agricultural and Forest Meteorology* 313, 108735. URL:
 716 <https://linkinghub.elsevier.com/retrieve/pii/S0168192321004214>, doi:[10.1016/j.agrformet.2021.108735](https://doi.org/10.1016/j.agrformet.2021.108735).
 717 Zhao, Y., Feng, D., Yu, L., Wang, X., Chen, Y., Bai, Y., Hernández, H.J., Galleguillos, M., Estades, C., Biging, G.S., Radke,
 718 J.D., Gong, P., 2016. Detailed dynamic land cover mapping of Chile: Accuracy improvement by integrating multi-temporal
 719 data. *Remote Sensing of Environment* 183, 170–185. URL: <https://linkinghub.elsevier.com/retrieve/pii/S0034425716302188>,
 720 doi:[10.1016/j.rse.2016.05.016](https://doi.org/10.1016/j.rse.2016.05.016).
 721 Zhou, K., Li, J., Zhang, T., Kang, A., 2021. The use of combined soil moisture data to characterize agricultural drought
 722 conditions and the relationship among different drought types in China. *Agricultural Water Management* 243, 106479. URL:
 723 <https://linkinghub.elsevier.com/retrieve/pii/S0378377420305965>, doi:[10.1016/j.agwat.2020.106479](https://doi.org/10.1016/j.agwat.2020.106479).
 724